The Weakening of the Stratospheric Polar Vortex and the Subsequent Surface Impacts as Consequences to Arctic Sea Ice Loss

YU-CHIAO LIANG,[a,b,c] YOUNG-OH KWON,[b] CLAUDE FRANKIGNOUL,[b,d] GUILLAUME GASTINEAU,[d] KAREN L. SMITH,[e] LORENZO M. POLVANI,[c,f,g] LANTAO SUN,[h] YANNICK PEINGS,[i] CLARA DESER,[j] RUONAN ZHANG,[k] AND JAMES SCREEN[l]

[a] *Department of Atmospheric Sciences, National Taiwan University, Taipei, Taiwan*
[b] *Woods Hole Oceanographic Institution, Woods Hole, Massachusetts*
[c] *Lamont-Doherty Earth Observatory, Columbia University, Palisades, New York*
[d] *Sorbonne Université, CNRS/IRD/MNHN, LOCEAN/IPSL, Paris, France*
[e] *Department of Physical and Environmental Sciences, University of Toronto Scarborough, Toronto, Ontario, Canada*
[f] *Department of Earth and Environmental Sciences, Columbia University, New York, New York*
[g] *Department of Applied Physics and Applied Mathematics, Columbia University, New York, New York*
[h] *Department of Atmospheric Science, Colorado State University, Fort Collins, Colorado*
[i] *Department of Earth System Science, University of California, Irvine, California*
[j] *National Center for Atmospheric Research Climate and Global Dynamics, Boulder, Colorado*
[k] *Department of Atmospheric and Oceanic Sciences and Institute of Atmospheric Sciences, Fudan University, Shanghai, China*
[l] *College of Engineering, Mathematics and Physical Sciences, University of Exeter, Exeter, United Kingdom*

(Manuscript received 4 March 2023, in final form 6 October 2023, accepted 18 October 2023)

ABSTRACT: This study investigates the stratospheric response to Arctic sea ice loss and subsequent near-surface impacts by analyzing 200-member coupled experiments using the Whole Atmosphere Community Climate Model version 6 (WACCM6) with preindustrial, present-day, and future sea ice conditions specified following the protocol of the Polar Amplification Model Intercomparison Project. The stratospheric polar vortex weakens significantly in response to the prescribed sea ice loss, with a larger response to greater ice loss (i.e., future minus preindustrial) than to smaller ice loss (i.e., future minus present-day). Following the weakening of the stratospheric circulation in early boreal winter, the coupled stratosphere–troposphere response to ice loss strengthens in late winter and early spring, projecting onto a negative North Atlantic Oscillation–like pattern in the lower troposphere. To investigate whether the stratospheric response to sea ice loss and subsequent surface impacts depend on the background oceanic state, ensemble members are initialized by a combination of varying phases of Atlantic multidecadal variability (AMV) and interdecadal Pacific variability (IPV). Different AMV and IPV states combined, indeed, can modulate the stratosphere–troposphere responses to sea ice loss, particularly in the North Atlantic sector. Similar experiments with another climate model show that, although strong sea ice forcing also leads to tighter stratosphere–troposphere coupling than weak sea ice forcing, the timing of the response differs from that in WACCM6. Our findings suggest that Arctic sea ice loss can affect the stratospheric circulation and subsequent tropospheric variability on seasonal time scales, but modulation by the background oceanic state and model dependence need to be taken into account.

SIGNIFICANCE STATEMENT: This study uses new-generation climate models to better understand the impacts of Arctic sea ice loss on the surface climate in the midlatitudes, including North America, Europe, and Siberia. We focus on the stratosphere–troposphere pathway, which involves the weakening of stratospheric winds and its downward coupling into the troposphere. Our results show that Arctic sea ice loss can affect the surface climate in the midlatitudes via the stratosphere–troposphere pathway, and highlight the modulations from background mean oceanic states as well as model dependence.

KEYWORDS: Stratospheric circulation; Ice loss/growth; Ensembles

1. Introduction

The rapid decline of Arctic sea ice, observed by routine satellite observations (Stroeve and Notz 2018), is a dominant consequence of anthropogenic climate change in the past four decades (Fetterer et al. 2017). Not only has Arctic sea ice extent decreased substantially (Comiso et al. 2008; Cavalieri and Parkinson 2012), but sea ice thickness has also reduced (Rothrock et al. 1999; Serreze and Stroeve 2015; Lindsay and Schweiger 2015; Kwok 2018). The seasonal evolution of Arctic sea ice has also undergone dramatic changes (Markus et al. 2009; Stroeve et al. 2014). Under future greenhouse gas emission scenario

Denotes content that is immediately available upon publication as open access.

Supplemental information related to this paper is available at the Journals Online website: https://doi.org/10.1175/JCLI-D-23-0128.s1.

Corresponding author: Yu-Chiao Liang, yuchiaoliang@ntu.edu.tw

DOI: 10.1175/JCLI-D-23-0128.1

simulations conducted by state-of-the-art global climate models participating in phase 6 of the Coupled Model Intercomparison Project (CMIP6; Eyring et al. 2016), the Arctic Ocean is projected to become nearly ice-free in boreal autumn by the middle of the twenty-first century (Notz et al. 2020). Highlighted in the Special Report on the Ocean and Cryosphere in a Changing Climate (IPCC 2019) and the Sixth Assessment Report of the Intergovernmental Panel on Climate Change (IPCC 2021), the retreat of Arctic sea ice has exerted profound impacts on local weather, ecosystems, and socioeconomic conditions (Grebmeier 2012; Jung et al. 2016) and has instigated rigorous debates on whether or not it has contributed to extreme weather events in North America and Eurasia (e.g., Barnes 2013; Cohen et al. 2014; Mori et al. 2014; Barnes and Screen 2015; Overland et al. 2015, 2016; Coumou et al. 2018; Blackport et al. 2019; Mori et al. 2019a,b; Screen and Blackport 2019a,b; Blackport and Screen 2020a,b; Cohen et al. 2020; Zappa et al. 2021; Smith et al. 2022).

Associated with the rapid loss of Arctic sea ice, a faster warming rate in the Arctic than in the tropics or the rest of the globe (Holland and Bitz 2003; Pithan and Mauritsen 2014; Goosse et al. 2018; Previdi et al. 2021; Taylor et al. 2021) is observed (Serreze and Francis 2006; Serreze et al. 2009; England et al. 2021; Chylek et al. 2022; Rantanen et al. 2022), recorded in paleoclimate proxies (Park et al. 2019), and simulated by several generations of climate models (Manabe and Wetherald 1975; Holland and Bitz 2003; Hahn et al. 2021; Chylek et al. 2022; Liang et al. 2020, 2021b; Rantanen et al. 2022; Wu et al. 2023; Zhou et al. 2023). This phenomenon, referred to as Arctic amplification (AA), implies a reduced north–south temperature gradient in the lower troposphere, which has the potential to dynamically link AA and the associated sea ice loss to changes in the jet stream, which in turn may modulate the amplitude and persistence of tropospheric planetary waves, leading to more frequent extreme events in the midlatitudes (Francis and Vavrus 2012, 2015; Cohen et al. 2014, 2018; Francis et al. 2018; Zou et al. 2021). Previous studies also proposed that amplified Arctic warming and sea ice loss give rise to a nearly barotropic response of the large-scale tropospheric circulation resembling the Northern Annular Mode (NAM; Thompson and Wallace 2000) at the hemispheric scale or the North Atlantic Oscillation (NAO; Hurrell 1995) over the North Atlantic sector (e.g., Deser et al. 2004; Singarayer et al. 2006; Seierstad and Bader 2009; Strey et al. 2010; Cassano et al. 2014; Screen et al. 2014; Wettstein and Deser 2014; Deser et al. 2016; Siew et al. 2020; Liang et al. 2021a). These suggested links to midlatitude atmospheric circulation changes and extremes have been referred to as the tropospheric pathway.

Another proposed mechanism linking AA and the midlatitude circulation builds upon the process of stratosphere–troposphere coupling (Baldwin and Dunkerton 2001) and is often called the stratospheric pathway (e.g., Jaiser et al. 2013; Cohen et al. 2014; Kim et al. 2014; Jaiser et al. 2016; Nakamura et al. 2016; Ruggieri et al. 2016; Xu et al. 2021, 2023). Distinct from the tropospheric pathway, Arctic sea ice loss along with the associated diabatic heating change (and possibly its gradients) first excites waves propagating upward into the stratosphere (Jaiser et al. 2013; Peings and Magnusdottir 2014a; Kim et al. 2014; Sun et al. 2015; Nakamura et al. 2016; Wu and Smith 2016; Zhang et al. 2018; Liang et al. 2021a; Sun et al. 2022), which weakens the stratospheric polar vortex via wave–mean flow interactions (Andrews et al. 1987). The perturbed stratospheric anomalies then migrate downward to the near surface with a projection onto the negative NAM/NAO pattern (Kidston et al. 2015; Polvani et al. 2017; Domeisen and Butler 2020; Domeisen et al. 2020; Baldwin et al. 2021; Liang et al. 2021b), although other studies showed that the impacts of stratosphere–troposphere coupling associated with sea ice loss may not always extend to the surface (e.g., Xu et al. 2023). Despite being dynamically feasible and statistically identifiable, such a chain of processes involves stratospheric and tropospheric circulations at multiple spatiotemporal scales in the presence of large internal variability, leading to small signal-to-noise ratios (Sun et al. 2015; Seviour 2017; Blackport and Screen 2019; Peings 2019; Liang et al. 2020; Sun et al. 2022). In addition, the short observational record may not provide robust statistical relationships between Arctic sea ice loss and stratospheric circulation changes. Thus, one needs to interpret causality with caution.

In an attempt to address the causality issue, a causal network technique has been applied to observational datasets to verify that stratosphere–troposphere coupling can indeed link Arctic sea ice loss, particularly that in the Barents–Kara Seas, to tropospheric circulation changes in midlatitudes (Kretschmer et al. 2016). An alternative, and more common, approach is to conduct numerical experiments using a general or global climate model (GCM) to explicitly single out the role of stratosphere–troposphere coupling and subsequent impacts on near-surface climate under specific Arctic sea ice loss conditions (e.g., Peings and Magnusdottir 2014a; Kim et al. 2014; Sun et al. 2015; Zhang et al. 2018; Sun et al. 2022). However, the GCM experiments conducted with different models show diverse stratospheric circulation responses to Arctic sea ice loss, with some modeling studies showing a weakened polar vortex (Kim et al. 2014; Nakamura et al. 2016) and others an intensified vortex (Cai et al. 2012; Scinocca et al. 2009; Screen et al. 2013; Sun et al. 2014; England et al. 2018) or negligible response (Dai and Song 2020; Peings et al. 2021; Smith et al. 2022; Sun et al. 2022). Such a wide range of sensitivity limits the utility of GCMs to improve our process-based understanding of the stratospheric responses to sea ice loss and the subsequent tropospheric climate impacts that are suggested by observations and reanalysis datasets. This diversity might be linked to the various strengths and spatial patterns of the sea ice forcing prescribed in the GCM experiments (Screen et al. 2018; Smith et al. 2019), the different background states (Chen et al. 2016; Smith et al. 2017; Labe et al. 2019) and strengths of eddy–mean flow interaction (Smith et al. 2022), and conflation of the sea ice–forced response with internal variability (e.g., Seviour 2017; Peings et al. 2021; Sun et al. 2022).

The Polar Amplification Model Intercomparison Project (PAMIP) of CMIP6 provides multiple GCM experiments with identical sea ice concentration (SIC) and sea surface temperature (SST) conditions, as well as large ensemble sizes, to investigate the causes and consequences of polar amplification (Smith et al. 2019). PAMIP, therefore, offers a useful test

bed for assessing Arctic–midlatitude linkages resulting from the response to sea ice loss via both the stratospheric and tropospheric pathways (e.g., Ronalds et al. 2020; Audette et al. 2021; Peings et al. 2021; Streffing et al. 2021; Smith et al. 2022; Sun et al. 2022). The ensemble size for the short (14 month) time-slice experiments was recommended to be 100 by the PAMIP protocol (see Table 1 of Smith et al. 2019), but several recent studies have indicated that more than 100 members are needed to sufficiently separate the sea ice–forced signals from internal atmospheric circulation variability (e.g., Labe et al. 2019; Liang et al. 2020; Peings et al. 2021; Sun et al. 2022). Moreover, the PAMIP protocol specified the same background mean SST states derived from the coupled model experiments of phase 5 of the Coupled Model Intercomparison Project (CMIP5) (Smith et al. 2019), overlooking the effects of different oceanic states on the atmospheric circulation responses to sea ice loss.

Previous studies have shown that the stratospheric circulation, its coupling to the troposphere, and the tropospheric circulation can be affected by SST anomalies associated with Atlantic multidecadal variability (AMV; Knight et al. 2005; Zhang et al. 2019), interdecadal Pacific variability (IPV; Henley et al. 2015), and their combination (Nishii et al. 2010; Woo et al. 2015; Omrani et al. 2014; Peings and Magnusdottir 2014b; Kren et al. 2016; Elsbury et al. 2019; Suo et al. 2022a,b; Omrani et al. 2022). Other studies also highlighted that the Arctic sea ice and the associated temperature responses can be modulated by AMV (e.g., Osborne et al. 2017; Li et al. 2018; Chen et al. 2021; Luo et al. 2022) or Pacific decadal variability (e.g., Screen and Francis 2016; Svendsen et al. 2018; Simon et al. 2022; Luo et al. 2022; Suo et al. 2022a,b). Hence, the concurrent phase shifts of AMV and IPV in the early twentieth century that occurred in conjunction with rapid Arctic warming (Tokinaga et al. 2017) suggest combined effects on Arctic climate change. Taken together, it would be also reasonable to constrain the SSTs to certain phases of AMV and IPV in the PAMIP experiments to investigate their modulating influence on the circulation response to Arctic sea ice loss via the stratospheric pathway.

In this study, we use the Whole Atmosphere Community Climate Model version 6 (WACCM6), which has a high-top configuration to better resolve stratospheric processes (Gettelman et al. 2019), to conduct the PAMIP time-slice atmosphere–land–ocean–sea ice coupled experiments. We carry out such fully coupled simulations instead of atmosphere-only experiments because some previous studies pointed out the importance of oceanic feedbacks in the atmospheric response to sea ice loss (e.g., Deser et al. 2016; Screen and Blackport 2019a; Screen et al. 2018). Unlike these previous studies, our focus is on the stratospheric response to Arctic sea ice loss and the subsequent impacts on near-surface climate. To address the issues of internal variability and background SST state dependence, both of which render the novelty of this study, we have increased the PAMIP protocol ensemble size to 200 members and incorporated combinations of different AMV and IPV SST states in the initial ocean conditions. The model configuration and experimental details are described in section 2. Section 3 presents the results according to the dynamical framework stratosphere–troposphere coupling, starting with tropospheric precursors including upward wave activity, followed by the stratospheric circulation response and, finally, the subsequent downward impacts on near-surface sea level pressure, temperature, and precipitation. We then analyze the modulating effects of combined AMV and IPV phases. Results from another GCM (IPSL-CM6A-LR; Boucher et al. 2020) are also examined to illustrate the model dependence issue. Discussion is provided in section 4, followed by a summary of results in section 5.

2. Data and methods

a. *Model descriptions*

In this study, we use WACCM6 of the Community Earth System Model version 2 (hereinafter CESM2-WACCM6; Danabasoglu et al. 2020) developed by the National Center for Atmospheric Research (NCAR). The WACCM6 adopts the finite-volume dynamical core (Lin and Rood 1997) with a 0.9° latitude × 1.25° longitude horizontal resolution and is the high-top version of the atmospheric component model of CESM2, which has 70 vertical levels from the surface to model top at 6×10^{-6} hPa (~140 km), in contrast to its low-top counterpart, the Community Atmosphere Model version 6 (CAM6; Danabasoglu et al. 2020), which has only 32 vertical levels with the model top at 2.26 hPa (~40 km). The WACCM6 has all the same physical parameterizations as CAM6, except the parameterization scheme of gravity waves (Gettelman et al. 2019): the orographical gravity wave drag parameterizations in WACCM6 and CAM6 are identical, but the parameters of frontal and convective parameterization in WACCM6 were changed to better characterize frontogenesis and the quasi-biennial oscillation (QBO). The WACCM6 has been shown to not only better simulate the stratospheric processes and circulation variability than CAM6, including sudden stratospheric warming events and the self-generated QBO (Gettelman et al. 2019; Ayarzagüena et al. 2020), but also better represent the tropospheric circulation compared to observations or reanalysis datasets, including storm tracks, stationary waves, and blocking in midlatitudes (Simpson et al. 2020).

To conduct the fully coupled PAMIP time-slice experiments, the WACCM6 is coupled to other model components of CESM2: the ocean component is the Parallel Ocean Program version 2 (POP2; Smith et al. 2010), the sea ice component is CICE version 5.1.2 (CICE5; Hunke et al. 2015), the land-ice component is the Community Ice Sheet Model Version 2.1 (CISM2.1; Lipscomb et al. 2019), the land component is the Community Land Model Version 5 (CLM5; Lawrence et al. 2019), and the river transport component is the Model for Scale Adaptive River Transport (MOSART; Li et al. 2013). More details on the fully coupled configuration can be found in Danabasoglu et al. (2020). We use the specified chemistry version of WACCM6, which does not resolve the interactive chemical contributions (Smith et al. 2014).

The second GCM used in this study is developed by L'Institut Pierre-Simon Laplace (IPSL) Climate Modeling Centre:

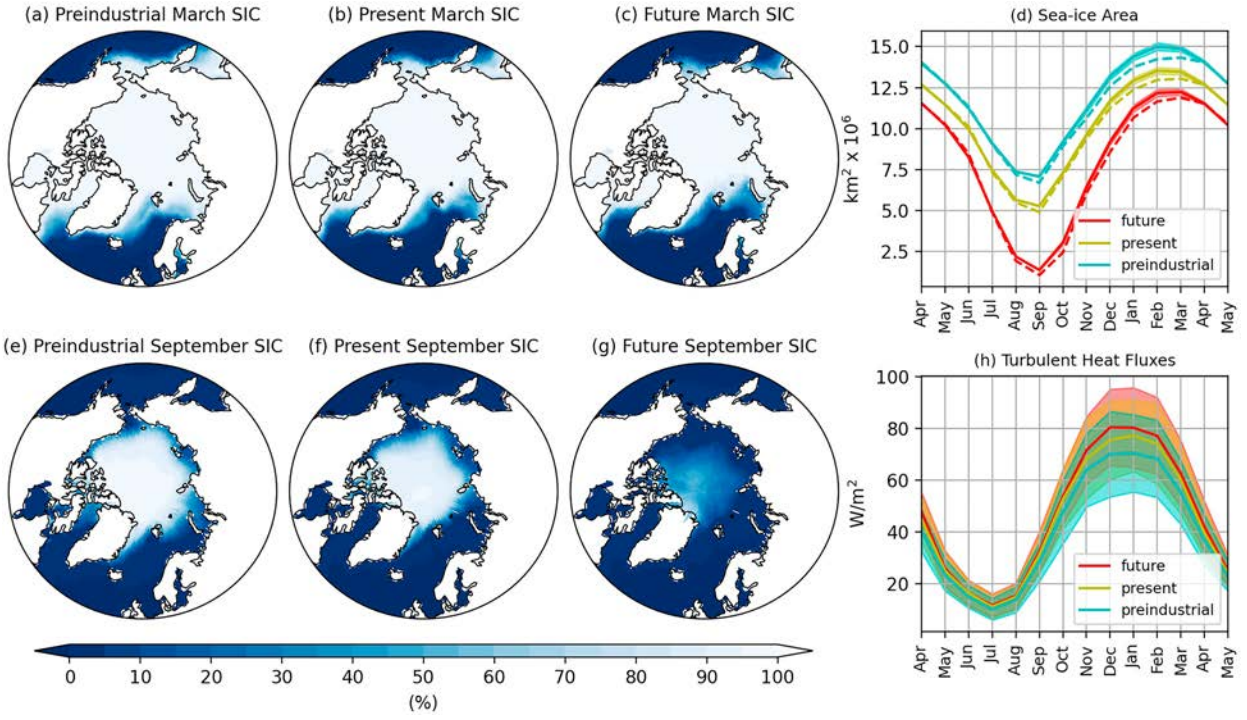

FIG. 1. March SICs averaged over 200 members for (a) preindustrial, (b) present, and (c) future time-slice coupled experiments and (e)–(g) the corresponding September SICs. (d) The evolution of sea ice area for each experiment during the integration period from April to May of the following year. (h) As in (d), but for turbulent heat flux from ocean to atmosphere averaged over the Arctic domain (60°–90°N). In (d) and (h), the thick lines represent the ensemble-mean values, while the color shadings delineate the two standard deviation ranges. In (d), the dashed lines are the target SIC values for the nudging.

the IPSL-CM6A-LR (Boucher et al. 2020). The atmospheric component is the LMDZ6A-LR (Hourdin et al. 2020) with a 1.3° latitude × 2.5° longitude horizontal resolution; it is also regarded as a high-top model as it has 79 vertical levels spanning from the surface to 0.01 hPa (~80 km). The land component is ORCHIDEE (Krinner et al. 2005). The LMDZ6-LR is coupled to the Nucleus for European Models of the Ocean version 3.6 (Madec et al. 2017), which includes the LIM3 sea ice component (Rousset et al. 2015; Vancoppenolle et al. 2009). More details about IPSL-CM6A-LR can be found in Boucher et al. (2020).

b. *PAMIP time-slice experiments*

We conduct the time-slice experiments with CESM2-WACCM6 following the PAMIP protocol [see experiments 2.1, 2.2, and 2.3 in Table 1 of Smith et al. (2019)]. The temporal integration period is from 1 April to 31 May of the following year, providing 14-month simulations. The CMIP6 radiative forcing is fixed at its year 2000 level during the integration period. We constrain the sea ice condition in each experiment by nudging both SIC and sea ice volume (SIV) toward the target preindustrial, present-day (hereinafter present), and future SIC and SIV conditions in the Northern Hemisphere (Smith et al. 2019; Peings et al. 2021), while the SIC and SIV in the Southern Hemisphere are constrained to be identical at present-day levels among the three experiments. The nudging constrains the sea ice thickness to be about 2 m in the Northern Hemisphere and 1 m in the Southern Hemisphere, as required by the PAMIP protocol. The SIV, therefore, is derived from the corresponding sea ice area multiplied by the thickness.

The present SIC conditions were obtained from the 1979–2008 climatology using the Hadley Centre Sea Ice and Sea Surface Temperature dataset (HadISST; Rayner et al. 2003). The preindustrial SIC values were generated from the 31 historical simulations of CMIP5 when the global mean temperature is close to 13.67°C, an estimation of the observational global mean temperature over the preindustrial period (Haustein et al. 2017). The future SIC conditions were obtained from the corresponding CMIP5 projections based on the 30-yr periods when the global mean temperature exceeds the preindustrial counterpart by 2°C under the representative concentration pathway 8.5 emissions scenarios (Hausfather 2020). The parallel sets of experiments carried out by IPSL-CM6A-LR use a similar nudging method, but it is implemented to only reach the target SIC, while the SIV is not directly constrained. The details and performance were documented in Simon et al. (2021).

The spatial distributions of March and September Arctic SICs in the time-slice runs are presented in Fig. 1. The future SIC is much smaller than the preindustrial and present SICs across the Arctic Ocean in September (Figs. 1e–g), while smaller future SICs appear mostly in the marginal ice zones, including the Sea of Okhotsk, Bering Sea, and Labrador Sea, in March (Figs. 1a–c). Examination of the Arctic sea ice area

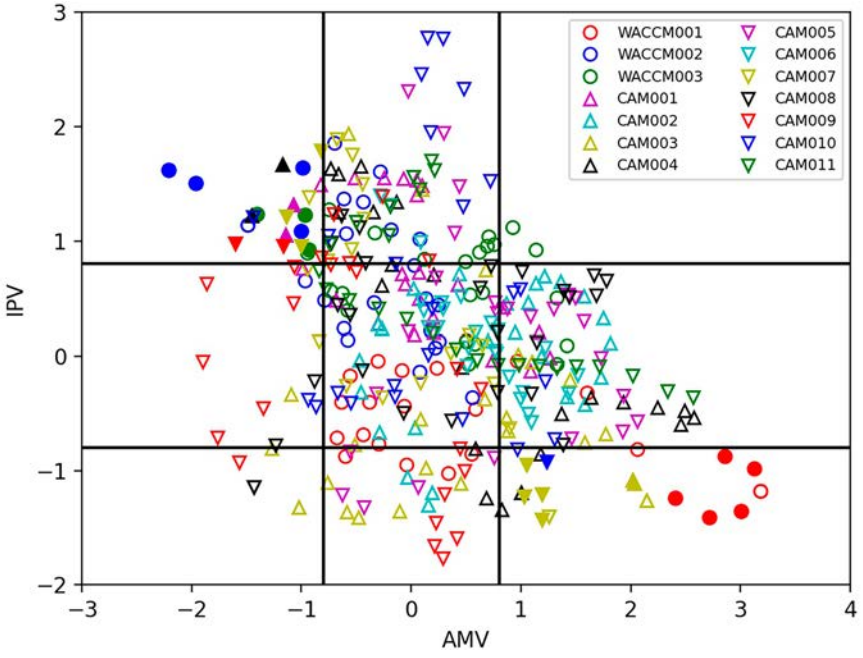

FIG. 2. The distribution of IPV and AMV phases during 1985–2014 from 3 CESM2-WACCM6 (circles) and 11 CESM2-CAM6 (triangles) historical simulations. The filled symbols are those samples used in the ICs of our experiments. See text for details.

(SIA) confirms that our nudging technique successfully constrains the simulated SICs (solid lines in Fig. 1d) toward the target (SIA; dashed lines in Fig. 1d) throughout the 14-month integration period. The smaller SIC and larger area of open water in the future runs enhance the upward surface turbulent heat fluxes averaged over the Arctic domain (60°–90°N) compared to the present and preindustrial runs, especially in autumn and winter when they reach their peak amplitude (Fig. 1h). This seasonality of turbulent heat fluxes is also seen in previous studies (e.g., Deser et al. 2020b, 2015; Sun et al. 2015; Sun et al. 2022). Hence, larger sea ice retreat in our simulations indeed promotes larger turbulent heat fluxes into the atmosphere as early as autumn, a factor that might initiate the subsequent stratospheric and tropospheric responses. In the following analyses, we refer to the variable (or response) of interest under "strong" sea ice forcing as that from the future runs minus the preindustrial runs, and under "weak" sea ice forcing as that in the future runs minus the present runs. Thus, the control or reference run is the future run. We also consider as "weak" sea ice forcing the present runs minus the preindustrial runs, and obtain similar results for stratospheric circulation responses (not shown). The corresponding figures for IPSL-CM6A-LR were documented in Simon et al. (2022, see their Fig. 1).

c. *IPV and AMV initial conditions*

To test if the atmospheric responses to Arctic sea ice loss are influenced by different phases of AMV and IPV, we choose the ocean initial conditions (ICs) with different AMV and IPV phases from existing CESM2 simulations and plot the oceanic state based on AMV indices against IPV indices (Fig. 2). We select 16 years with AMV− and IPV+ phases (hereinafter AMV−/IPV+) and 14 years for AMV+ and IPV− (hereinafter AMV+/IPV−) from 3 CESM2-WACCM6 and 11 CESM2-CAM6 historical simulations, which were conducted following the CMIP6 protocol from 1850 to 2014 (Danabasoglu et al. 2020), using the 1985–2014 period (filled solid symbols in Fig. 2). Other combinations of AMV and IPV states (i.e., AMV+/IPV+ and AMV−/IPV−) could not be sufficiently sampled with the available historical simulations (Fig. 2). The SST variability in the CESM2-CAM6 and CESM2-WACCM6 historical simulations is comparable (Fig. S5 in the online supplemental material), justifying that ICs are sampled from both models. The AMV state is determined by a normalized AMV index, defined as the annual mean SST averaged over 0°–60°N (North Atlantic domain) minus the annual global-mean SST, smoothed with a 10-yr low-pass filter [based on the index calculated in Kerr (2000) and in Enfield et al. (2001) with slight modification in the chosen domain and window length for low-pass filter]. If the AMV index is larger (smaller) than 0.8 (−0.8), we select it as an AMV+ (AMV−) state. For the IPV, we follow Henley et al. (2015) to calculate the tripolar SST index and determine an IPV+ (IPV−) state when the normalized index is larger (smaller) than 0.8 (−0.8). We choose 0.8 at the threshold for these indices in order to increase the sample size.

The ocean initial state for the full depth is sampled on 1 April for each of the 16 AMV−/IPV+ and 12 AMV+/IPV− simulations described above. The ICs for land and atmosphere are obtained from present-day mean states of CESM2-WACCM6 historical simulations. In addition, we perturb in each case the initial atmospheric temperature fields

with small values (the so-called pertlim method; Kay et al. 2015; Deser et al. 2020) to construct a total of 100 ICs for AMV+/IPV− and AMV−/IPV+ cases. This approach provides the ICs to initiate our 200-member sea ice loss experiments. We verified that the initial SSTs in our experiments persist into winter with consistent AMV and IPV SST patterns (see Figs. S1–S4). A similar procedure is performed in sampling ICs for IPSL-CM6A-LR.

d. *Random resampling procedure*

Recent studies based on PAMIP experiments found that sampling fluctuations due to internal variability are large (e.g., Peings et al. 2021; Smith et al. 2022; Sun et al. 2022). For example, Sun et al. (2022) showed that even the sign of the stratospheric circulation response to Arctic sea ice loss can be opposite between the first and the second halves of a 200-member ensemble (see Fig. 3a of Sun et al. 2022). Hence, the uncertainty due to internal variability must be robustly estimated. A commonly used method is the random sampling (bootstrapping) procedure (Mudelsee 2010; Pedregosa et al. 2011), which constructs "resamples" from ensemble members (e.g., Oehrlein et al. 2019; Liang et al. 2022a; Sun et al. 2022). In this study, we randomly sample 200 members from the merged sample of preindustrial, present, and future runs for 10 000 times with replacement. To obtain the distributions of 10 000 ensemble means for the stratospheric responses under strong and weak sea ice forcings, we take their difference and average them over the 200 resampled members. Results are similar if we change the resampled size to 100.

e. *Field significance*

The statistical significance of the difference maps may be overestimated if one simply uses the standard two-tailed Student's t test at each grid point (i.e., local significance; Livezey and Chen 1983; Wilks 2016). To address this issue, Wilks (2016) introduced the concept of "field significance," which constrains the false discovery rate (FDR). Recent PAMIP studies have used the field significance to determine the robustness of sea ice loss–forced circulation changes (e.g., Peings et al. 2021; Sun et al. 2022). We choose the test level $\alpha_{FDR} = 0.1$ to achieve a global test level $\alpha_{FDR} = 0.05$ for a spatial decorrelation scale of $\sim 1.54 \times 10^3$ km (see Fig. 4 in Wilks 2016), as derived from the spatial autocorrelation of geopotential height field at 500 hPa (Polyak 1996). We also apply the field significance to the height–time domain with $\alpha_{FDR} = 0.1$ (D. S. Wilks 2019, personal communication).

3. Results

a. *Sea ice loss enhances stratosphere–troposphere coupling*

We begin by examining the time evolution of the stratospheric and tropospheric responses to Arctic sea ice loss. Figures 3a and 3b show the time evolution of the polar cap–averaged (65°–90°N) geopotential height (hereinafter Z) responses from 1000 to 1 hPa, averaged over the 200 ensemble members for strong and weak sea ice forcings, respectively, from 1 September to the following 1 April. Clearly, the strong sea ice forcing gives rise to stronger negative polar cap Z responses in both the stratosphere and troposphere in autumn and winter, indicating that a more pronounced stratosphere–troposphere coupling is established by greater sea ice loss. Under strong sea ice forcing, the tropospheric precursors emerge in October and begin to migrate upward into the stratosphere in the middle of November (Fig. 3a). In contrast, the upward branch is absent or not statistically significant in late November and December under weak sea ice forcing, showing a decoupling between the troposphere and stratosphere in autumn and early winter (Fig. 3b).

Since the stratospheric polar vortex can be perturbed by vertical wave activity fluxes from the troposphere (Polvani and Waugh 2004), we next examine the Eliassen–Palm (EP) fluxes (Edmon et al. 1980), which manifest the vertical and meridional propagation of Rossby waves in the vertical–latitude coordinate, in response to sea ice forcings in November and December (Fig. 4). Stronger and enhanced upward EP fluxes are instigated in the lower troposphere and propagate vertically into the lower stratosphere (~50 hPa) between 60° and 80°N in late November when the sea ice forcing is strong (Fig. 4a). After entering the stratosphere, the EP fluxes are refracted equatorward. As the convergence (divergence) of the EP fluxes is a useful measure to diagnose the resultant zonal-mean zonal wind deceleration (acceleration) via the wave–mean flow interaction (Andrews et al. 1987), we superimpose the zonal-mean zonal wind responses in Fig. 4. We find reduced winds in the lower stratosphere (50–10 hPa) between 60° and 80°N and in the higher stratosphere (10–1 hPa) centered around 40°N in the strong ice forcing case (Fig. 4a), consistent with the EP flux convergence. The dipolar zonal-wind feature in the high stratosphere (10–1 hPa) is also largely explained by the wind tendency induced by the divergence and convergence of EP fluxes. In contrast, fewer upward EP fluxes enter the stratosphere in late November when the sea ice forcing is weak (Fig. 4e), and they have no field significant influence on the zonal-mean zonal wind and do not lead to reduced stratospheric circulation. In early and mid-December, the EP flux and zonal wind responses remain largely similar to those in late November, but they become somewhat weaker under strong SIC forcing (Figs. 4b,c). In late December, enhanced EP fluxes instigated in the midtroposphere give rise to a reduced stratospheric circulation with wider extent (Fig. 4d). For weak SIC forcing, more EP fluxes enter the stratosphere and weaken the zonal winds there only after mid-December (Figs. 4g,h). These results clearly illustrate that the stronger sea ice forcing more effectively influences the stratospheric circulation in November and December via vertical wave propagation and eddy–mean flow interaction than the weaker sea ice forcing.

Focusing on the stratospheric circulation responses in December, when they attain maximum strength (recall Figs. 3a,b), we further analyze the polar cap Z at 10 hPa (hereinafter Z10; yellow dashed lines in Figs. 3a,b) under the strong and weak sea ice forcings. Here, we aim to estimate how the stratospheric response varies with the strength of sea ice forcing and also to determine its robustness. Figure 3c shows the

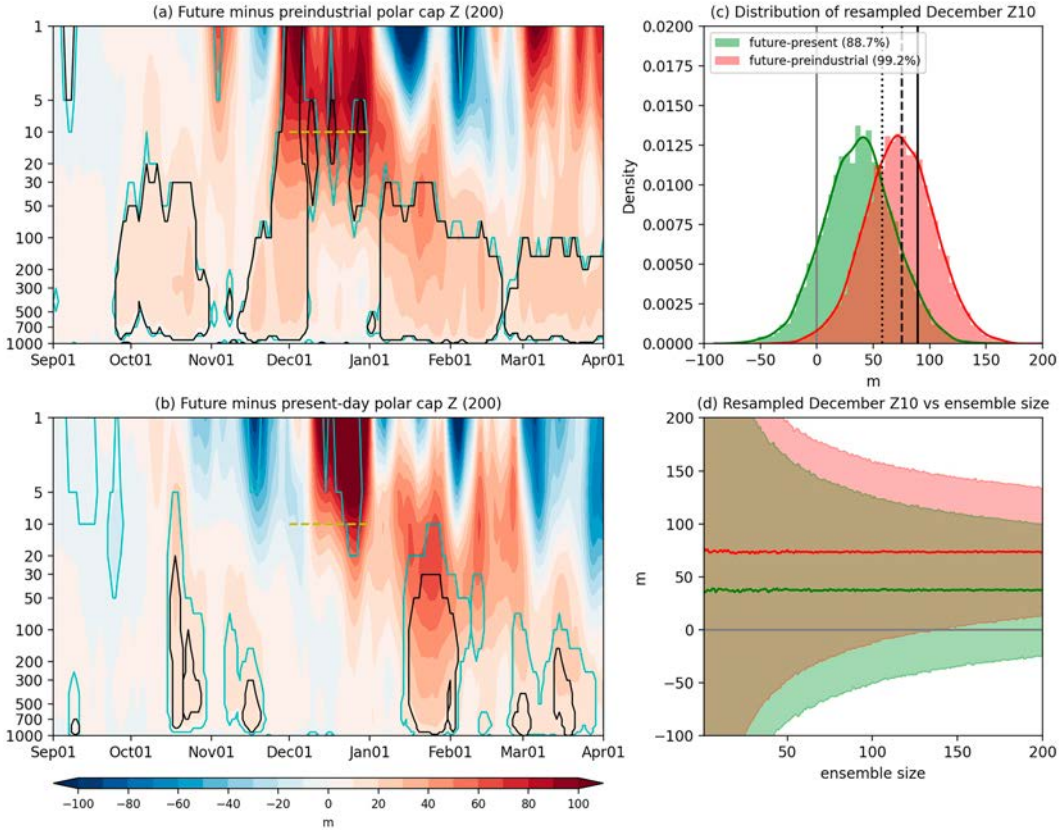

FIG. 3. Evolution of polar cap–averaged geopotential height (Z) response from 1 Sep to 1 Apr of the following year under (a) strong sea ice forcing and (b) weak sea ice forcing. The polar cap is defined as the region covering 65°–90°N. In (a) and (b), the black contours denote the field significance, while the cyan contours show the 5% local significance. The yellow dashed lines highlight the 10-hPa level in December. (c) Resampled distributions of December geopotential height response at 10 hPa (Z10) under strong (red distribution) and weak (green distribution) sea ice forcings. The dashed, dotted, and solid vertical lines are the ensemble-mean Z10 responses under strong sea ice forcing based on members 1–100, 51–150, and 101–200, respectively. The percentage of 10 000 resampled 200-member averages above zero is given in the legend. (d) Resampled ensemble-mean December Z10 responses (solid line) and the two standard deviation envelope (color shading) as a function of ensemble size; see text for details.

distributions of resampled ensemble means (section 2d). The strong sea ice forcing results in a Z10 increase by 74 ± 61 m (mean ± two standard deviations), corresponding to a decelerated polar vortex, whereas the weak sea ice forcing only enhances Z10 by 37 ± 62 m. Thus, the stratospheric response is twice as large in the strong sea ice forcing case than the weak one, while the uncertainty ranges due to internal variability are comparable. About 99% of the resamples under strong sea ice forcing are larger than zero (the red distribution), as compared to only 88% under weak sea ice forcing (the green distribution).

To further estimate the effect of internal variability, we compare two standard deviations of the resampled Z10 distributions (hereinafter 2xSD), containing about 95% of the resamples, and obtain 61 and 62 m for the strong and weak sea ice forcing runs, respectively. The similar values indicate that the effect of internal variability is insensitive to the strength of sea ice forcing. Comparison with the ensemble-mean Z10 responses in the strong and weak sea ice forcing cases, which are 74 and 37 m, respectively, leads to signal-to-noise ratios of 1.18 and 0.66, respectively, reflecting that the forced stratospheric responses are relatively small compared to the internal variability, as documented in previous studies (e.g., Liang et al. 2021b; Smith et al. 2022; Sun et al. 2022). Another perspective is to analyze the amplitude of internal variability as a function of the ensemble size. We are particularly interested in how many ensemble members are needed for the lower bound of the 2xSD envelope to be larger than zero (Fig. 3d). For the strong sea ice forcing case, 138 members are needed, while for the weak sea ice forcing case, 200 members are not enough. We, thus, conclude that in December, more than ~140 members are needed to single out with 95% confidence the sign of the forced stratospheric signal from the internal variability when the sea ice forcing is strong, and more than 200 members are needed if the sea ice forcing is weak. If we lower the confidence level to 90%, ~90 members are needed for strong SIC forcing, but still more than 200 members are required for weak SIC forcing. Hence, the necessary number

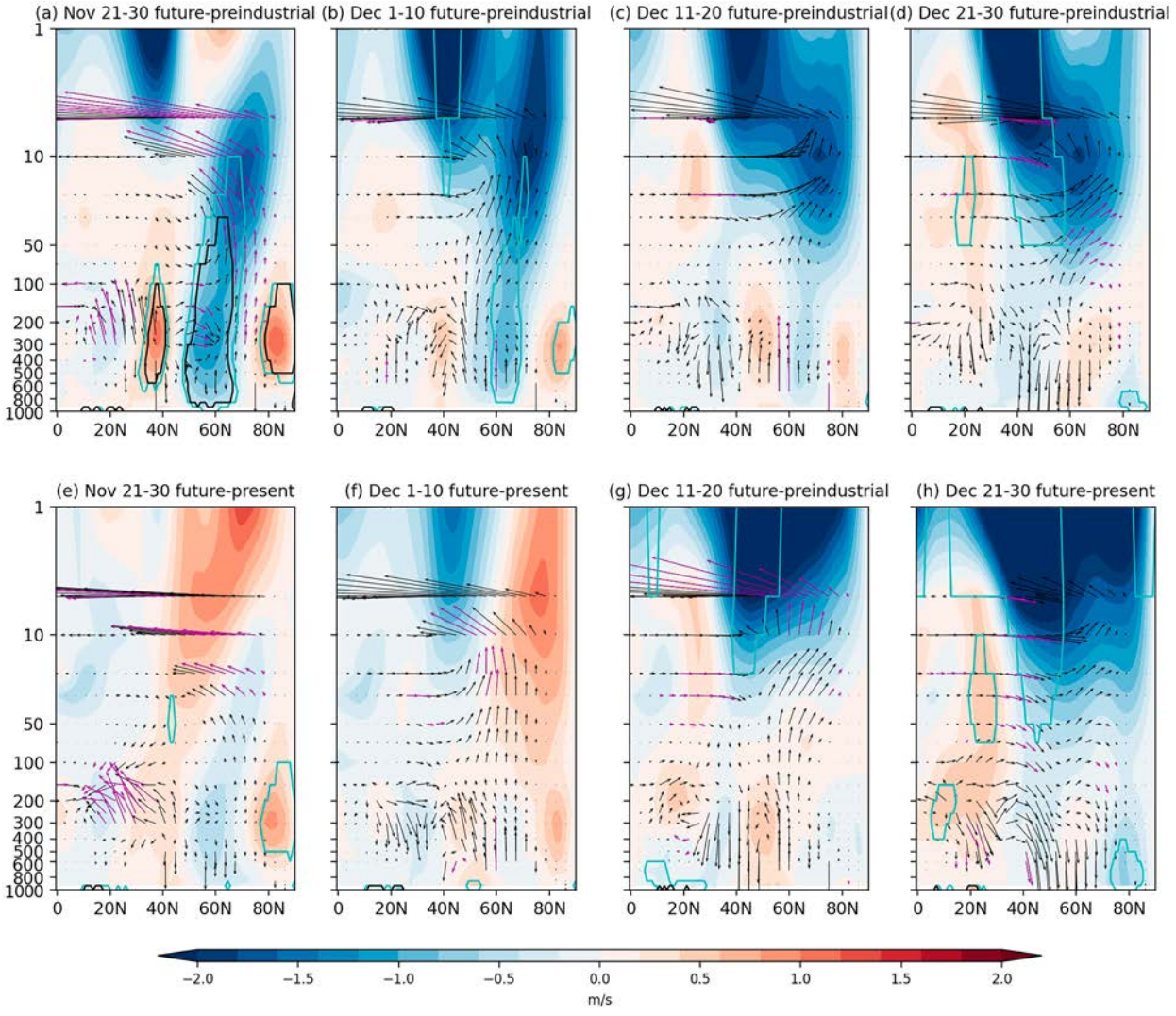

FIG. 4. Late November (21–30 Nov) EP fluxes (arrows) and zonal-mean zonal wind (color shadings) under (a) strong sea ice forcing and (e) weak sea ice forcing. The remaining panels are as in (a) and (e), but for (b),(f) early December (1–10 Dec), (c),(g) mid-December (11–20 Dec), and (d),(h) late December (21–30 Dec). The black contours denote field significance for zonal winds, and the cyan contours denote the 5% local significance based on the Student's *t* test. The magenta vectors are at 5% significance level based on the Student's *t* test for either vertical or meridional components.

for the weak SIC forcing runs is larger than recommended by the PAMIP protocol (Smith et al. 2019).

While the polar cap Z provides an overview of the stratosphere–troposphere response to the sea ice forcing, further insight can be obtained by examining the spatial distributions of the Z response. We first investigate the December response pattern of Z at 300 hPa (hereinafter Z300) and decompose it into wavenumber-1 and wavenumber-2 components. Following the framework of constructive and destructive interference (e.g., Smith and Kushner 2012; Sun et al. 2015; Sun et al. 2022), we find that for the wavenumber-1 component, both strong and weak SIC forcings give constructive interference (Fig. S6). For the wavenumber-2 component, strong SIC forcing produces more constructive features than weak SIC forcing, in particular over the northern European and Siberian sectors (Fig. S7). This analysis confirms that the strong SIC forcing gives rise to a circulation response pattern in December that favors upward EP fluxes and stronger stratosphere–troposphere coupling (Smith and Kushner 2012). We then consider the January–February response patterns of Z at 50 hPa (hereinafter Z50), 500 hPa (hereinafter Z500), and SLP (Fig. 5). In the stratosphere, a large and significant Z50 increase reaching 60 m occurs around Greenland for strong sea ice forcing (Fig. 5a). By contrast, the Z50 response to weak sea ice forcing extends over the whole polar region with the maximum over Greenland but lacks field significance (Fig. 5b). Therefore, the stratospheric polar vortex weakening (or meandering from north to south) is more confined in the

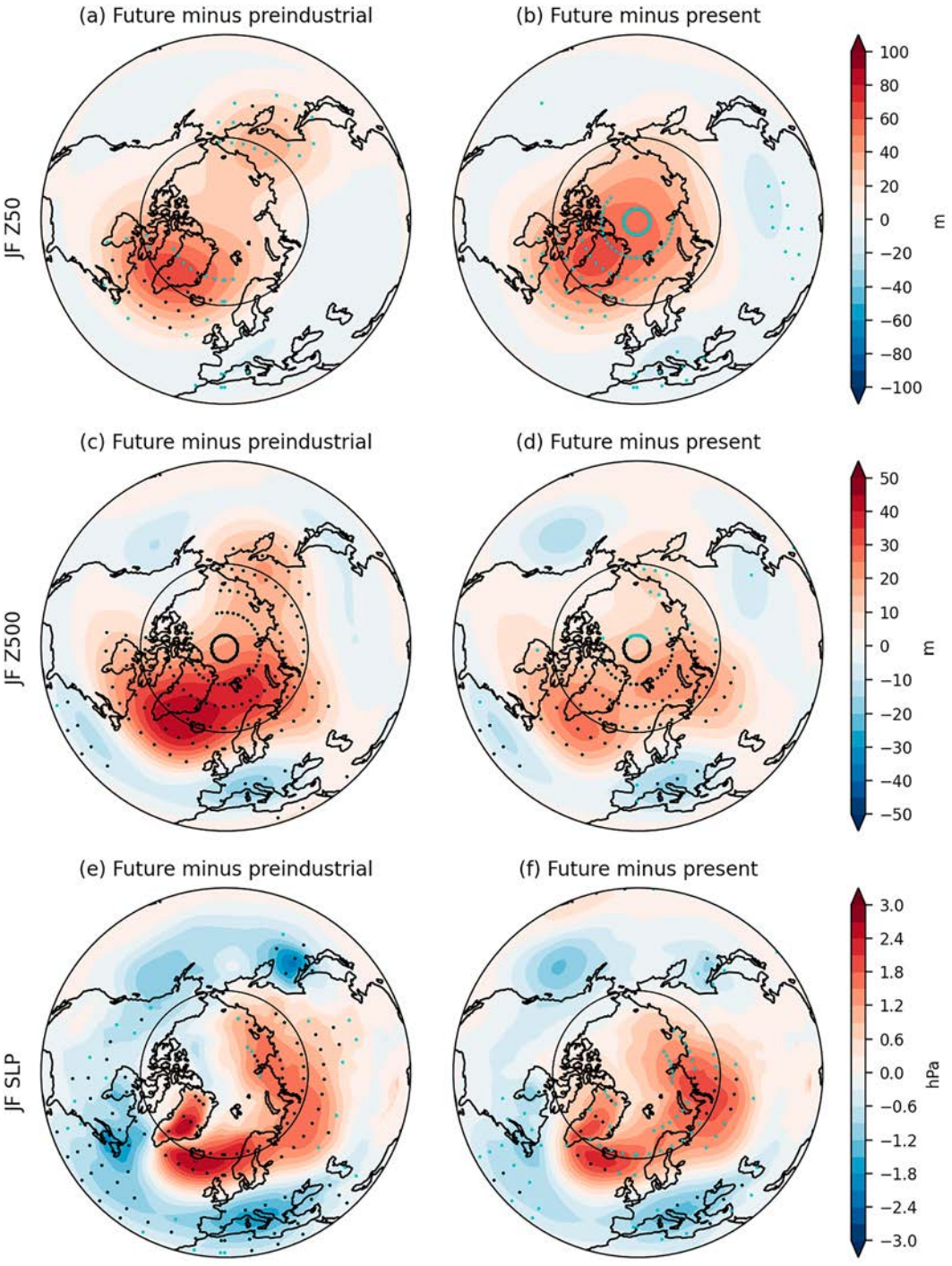

FIG. 5. January–February mean Z50 responses under (a) strong sea ice forcing and (b) weak sea ice forcing. The remaining panels are as in (a) and (b), but for (c),(d) Z500 and (e),(f) SLP. The black dots denote the field significance, while the cyan dots denote the 5% local significance.

North Atlantic sector under strong sea ice forcing. In the middle troposphere, Z500 increases in both cases over the broader region (Figs. 5c,d), but strong sea ice forcing gives rise to stronger Z500 increases above the North Atlantic and northern Siberia. Significant responses are also seen in the SLP, indicating nearly barotropic circulations, again with stronger magnitude for strong sea ice forcing (Figs. 5e,f). The dipolar SLP pattern in the North Atlantic largely resembles a negative NAO pattern, which has imprints on the wind and precipitation (Hurrell et al. 2003; section 3b). Over northern Siberia,

enhanced SLP appears in both weak and strong sea ice forcing cases (Figs. 5e,f). For strong sea ice forcing, the increased SLP extends from eastern Europe to northeastern Siberia, penetrating into central China. In contrast, weak sea ice forcing produces SLP increases mostly concentrated in the Ural Mountain regions, resembling a Ural blocking circulation (Peings 2019).

To summarize, in our CESM2-WACCM6 simulations, a stronger stratosphere–troposphere coupled response during late autumn and winter is produced by strong sea ice forcing compared to weak sea ice forcing. Sea ice loss reduces SLP during November over the Arctic and excites more upward planetary waves into the stratosphere. Then, via wave–mean flow interactions, the convergence of wave activity reduces the strength of the stratospheric polar vortex, peaking in December. In January and February, the perturbed stratospheric signal gradually migrates downward throughout the troposphere. Such a chain of events is not seen as robustly under weak sea ice forcing, perhaps because of the smaller signal-to-noise ratio.

b. *Impacts on the near-surface circulation, precipitation, and temperature*

After the stratospheric polar vortex is perturbed, it can trigger subsequent downward migration and affect surface climate (Baldwin and Dunkerton 2001). In our simulations, indeed, after the stratospheric polar cap weakens during December, the signal gradually descends to the lower troposphere and near surface in January and February, affecting zonal wind at 850 hPa (U850 hereinafter), precipitation, and surface air temperature (SAT) as shown in Fig. 6. We first focus on the North Atlantic sector where the January–February mean responses are of largest magnitude and statistical significance. Consistent with the negative NAO-like responses shown earlier (Figs. 5e,f), U850 is displayed toward the north of polar jet stream associated with weakened polar vortex (Kidston et al. 2015) and weakened in the downstream regions of the mean eddy-driven jet, and possibly results in reduced storm-track activity (Seierstad and Bader 2009; Harvey et al. 2014), as evidenced by a precipitation decrease over the eastern North Atlantic. The response patterns of U850 and total precipitation are largely similar in the weak sea ice forcing case, but with smaller magnitude and less statistical significance (Figs. 6b,d).

Localized warming occurs above large sea ice loss regions, including the Barents–Kara Seas, the western Greenland Sea, Hudson Bay, the Bering Strait, and the Sea of Okhotsk (Figs. 6e,f). In these regions, the total precipitation also increases (Figs. 6c,d) as a result of enhanced evaporation due to more open water. Again, the amplitudes are stronger for strong sea ice forcing. We also notice that the "warm Arctic–cold Eurasia" pattern, suggested to be produced by stratosphere–troposphere coupling (e.g., Zhang et al. 2018; Xu et al. 2021), does not appear in the SAT responses to sea ice loss in our CESM2-WACCM6 simulations (Figs. 6e,f).

It is noted that, although these near-surface responses are consistent with the imprints of the downward migration of stratospheric responses, they could also contain confounding effects due to the thermodynamical and dynamical processes within the troposphere, as well as concurrent sea ice loss impacts in late winter and early spring.

c. *Modulation by AMV and IPV states*

The macroperturbations of the ocean initial conditions in our experiments allow us to investigate whether certain AMV and IPV combined states affect the coupled stratosphere–troposphere response to sea ice loss and subsequent impacts on near-surface climate. We combine the two 100-member ensemble atmospheric responses for the strong and weak SIC forcing cases initialized with the AMV+/IPV− state to increase the ensemble size to 200 (and similarly for the AMV−/IPV+ state), because almost no 5% significant difference between ensemble-mean responses for strong and weak forcings can be found with only 100 ensemble members, consistent with the threshold in Fig. 3. To validate the mixture of the strong and weak responses and the linear additivity, we compare the two sets of circulation responses. The spatial distributions of them are largely similar (Figs. S8–S10). Thus, we interpret the 200-member combined response as the "median" response.

Figures 7a and 7b show the ensemble-mean polar cap Z responses to sea ice loss under the AMV+/IPV− and AMV−/IPV+ states, respectively. The AMV+/IPV− state gives rise to a statistically robust downward migration during late December and January (Fig. 7a), whereas the AMV−/IPV+ state does not. Neither state exhibits clear upward migration of tropospheric signals to the stratosphere in November and early December. We also look at the difference between the ensemble-mean polar cap Z responses under the AMV+/IPV− and AMV−/IPV+ states (Fig. 7c) to investigate the responses that are distinct in the two different oceanic background states. No statistically significant difference occurs in the stratosphere between November and most of March, except for a broad lowering between late January and early February. However, there are more significant signals in the lower troposphere, suggesting that the modulation effect particularly matters in the lower troposphere in the sense of polar-cap average. Nonetheless, the polar-cap averages could overlook the spatial structure of stratospheric and tropospheric responses and their coupling. Thus, we next investigate the modulation by AMV and IPV states of the spatial patterns of Z50, Z500, and SLP responses to sea ice loss (Fig. 8).

The AMV+/IPV− state produces two extended Z50 ridge patterns over the North Atlantic and northeastern Europe (Fig. 8a), which descend to 500 hPa (Fig. 8d) and to the near-surface level to affect SLP (Fig. 8g). However, the SLP responses over Siberia are statistically insignificant. The SLP responses are also less significant than Z500 or Z50 over the North Atlantic, indicating that the signals become less robust and weaker in the near surface than in the middle troposphere and stratosphere. The AMV−/IPV+ state gives rise to SLP responses with more statistical significance in the North Atlantic (Fig. 8h), which resemble the negative NAO pattern, and extends to the middle troposphere at

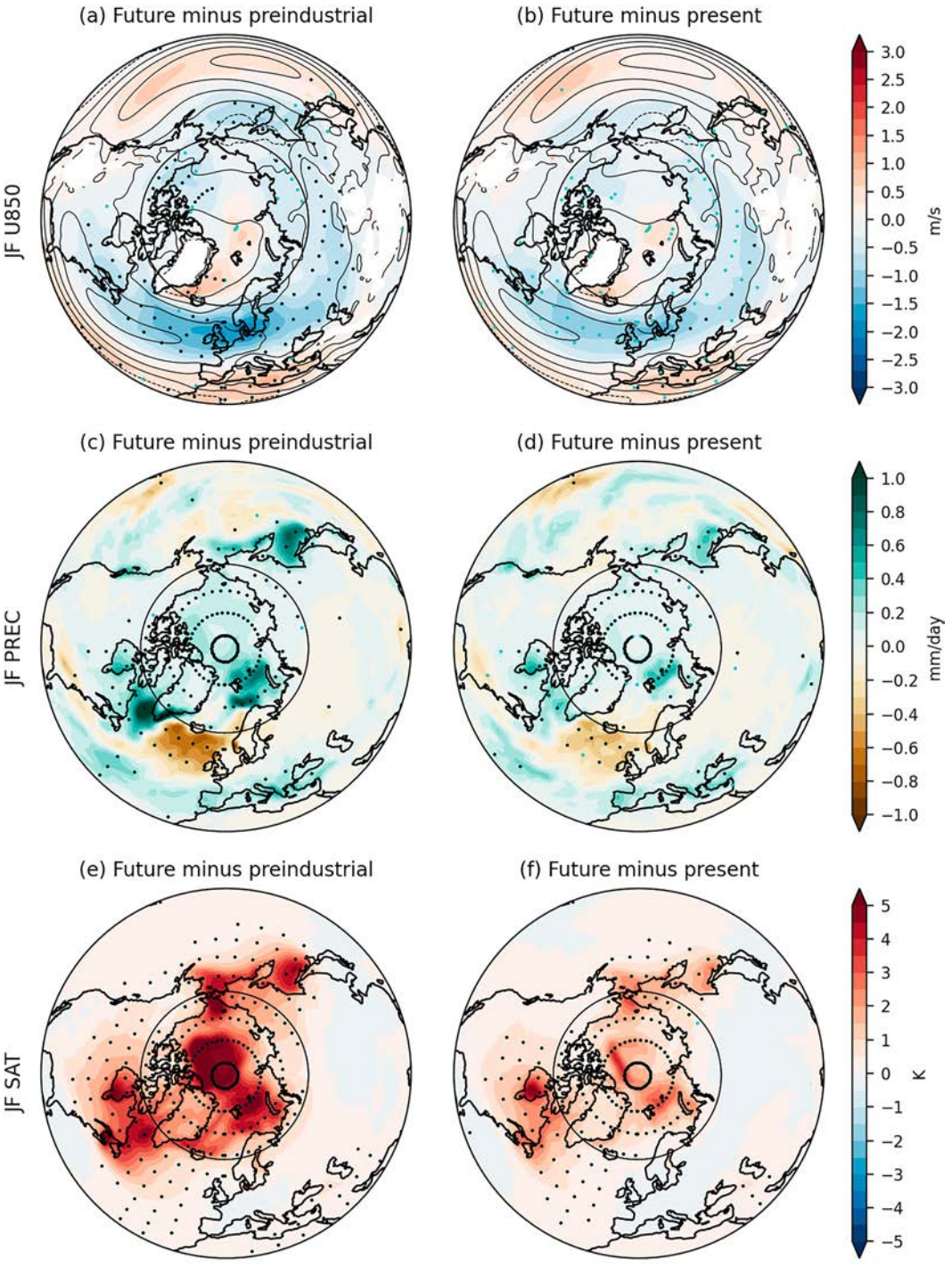

FIG. 6. January–February mean U850 responses under (a) strong sea ice forcing and (b) weak sea ice forcing. The remaining panels are as in (a) and (b), but for (c),(d) total precipitation (convective plus large-scale) and (e),(f) SAT. The black dots denote the field significance, while the cyan dots denote the 5% local significance. The black contours in (a) and (b) denote the climatological mean U850 (contour interval of 4 m s^{-1}; solid contours for positive values and dashed contours for negative values).

500 hPa (Fig. 8e) and the lower stratosphere (Fig. 8b). The corresponding U850 and total precipitation are shown in Fig. 9, which also indicates that the SAT response is not strongly modulated by AMV/IPV states, with similar SAT responses localized to the regions of maximum sea ice loss (Figs. 9g,h), and differences that are primarily significant over the North Atlantic subpolar gyre, consistent with a positive AMV state.

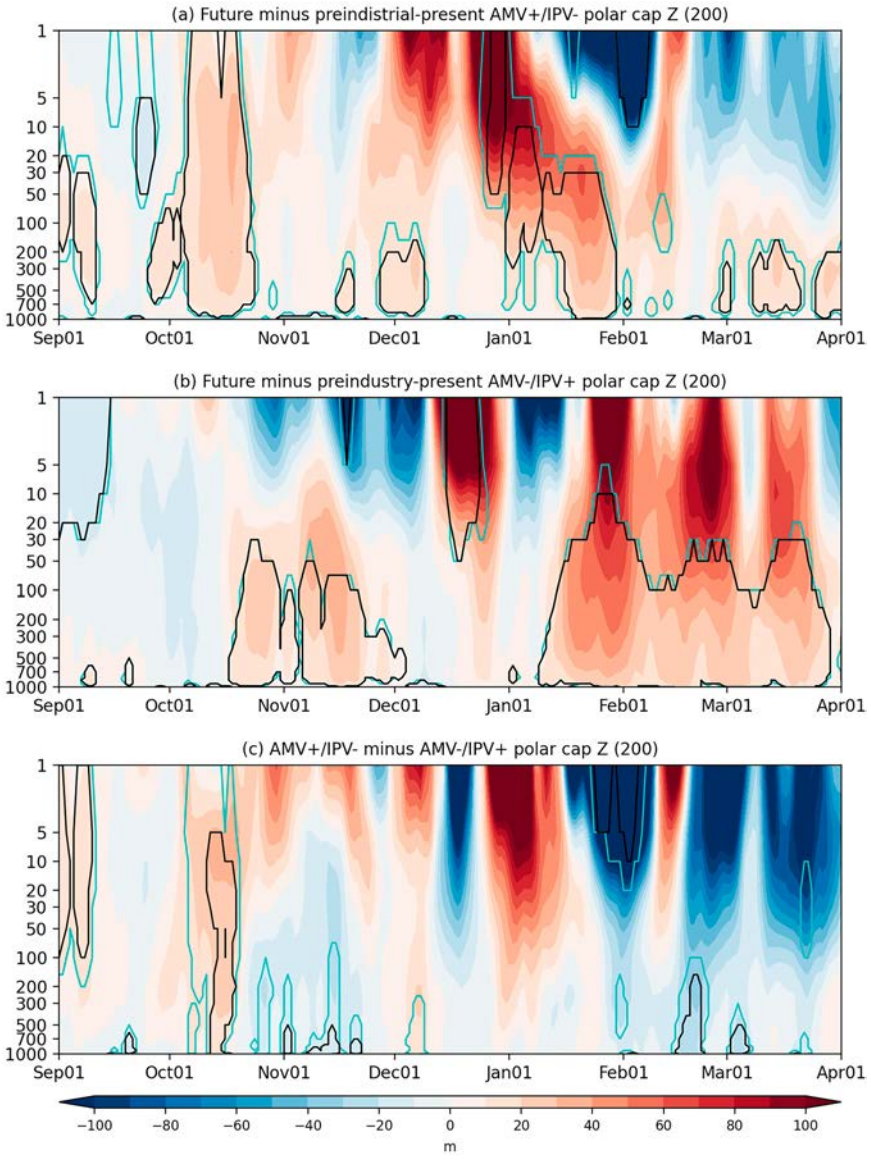

FIG. 7. Evolution of polar cap–averaged Z response to Arctic sea ice loss from 1 Sep to 1 April of the following year under (a) AMV+/IPV− and (b) AMV−/IPV+ states. Here, the responses to strong and weak sea ice forcings are combined. (c) The difference between (a) and (b). The black contour lines denote the field significance, while the cyan contour lines denote the 5% local significance.

The response difference plots with statistical significance reveal that the most critical circulation response associated with different oceanic background states resides in the North Atlantic sector, particularly in the middle and lower troposphere (Figs. 8f,i). The AMV+/IPV− state tends to produce stronger Z500 and SLP in the North Atlantic, along with a slightly northward shift and strengthening of Atlantic jet (Fig. 9c) and reduced precipitation west of Spain (Fig. 9f). The North Atlantic, thus, is the key region where different oceanic background states could effectively modulate the atmospheric responses to Arctic sea ice loss.

d. Model dependence

Although the sequence and processes of stratosphere–troposphere coupling and surface climate impacts forced by Arctic sea ice loss are dynamically feasible and statistically significant in CESM2-WACCM6, they could differ in other climate models, as suggested in previous studies (e.g., Screen et al. 2018; Smith et al. 2019). We thus consider another set of simulations produced with IPSL-CM6A-LR, which follow the same PAMIP protocol (Simon et al. 2022). In this model, the stratosphere–troposphere coupling and the enhanced polar cap Z are also clearly detected under strong sea ice forcing,

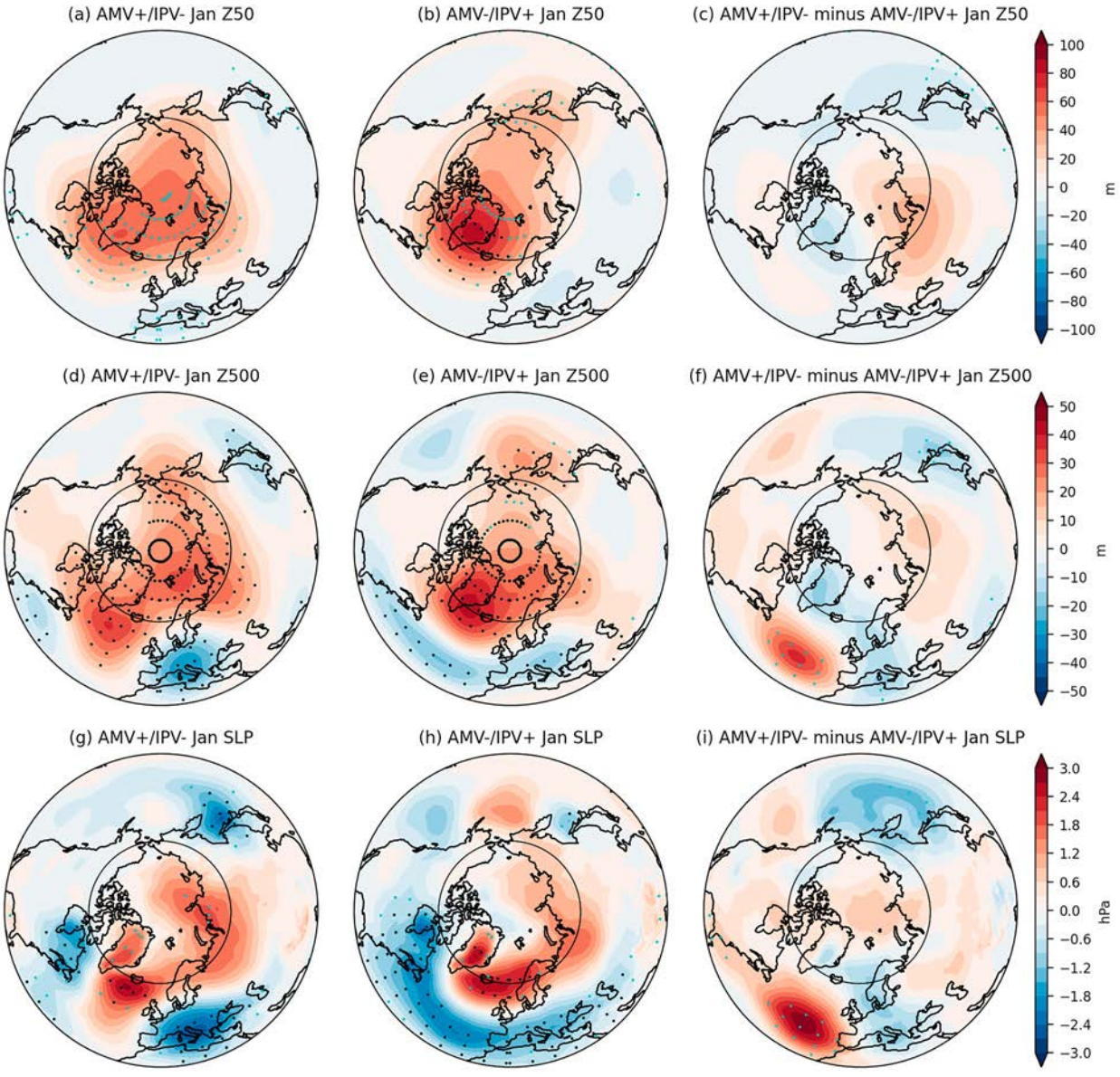

FIG. 8. January (a),(b) Z50, (d),(e) Z500, and (g),(h) SLP responses to sea ice forcing during AMV+/IPV− and AMV−/IPV+ states, respectively. Also shown are (c) the difference between (a) and (b); (f) the difference between (d) and (e); and (i) the difference between (g) and (h). Here, the responses to strong and weak sea ice forcings are combined. The black dots denote the field significance, while the cyan dots denote the 5% local significance.

but the polar cap Z perturbation in the stratosphere peaks during February (Fig. 10a), much later than the December peak in CESM2-WACCM6 (Fig. 4a). There is also no evidence of stratosphere–troposphere coupling under the weak sea ice forcing (Fig. 10b). Therefore, the temporal evolution of the stratosphere–troposphere coupling forced by sea ice loss is subject to substantial model dependence, possibly due to different mean states or seasonality of stratospheric and tropospheric circulations.

We also repeat our random resampling analysis for the IPSL model. Figure 10c shows the distributions of resampled ensemble means of Z10 for the strong and weak sea ice forcing cases. The strong sea ice forcing results in an 83-m increase in Z10, with 99% of the resamples larger than zero (the red distribution in Fig. 10c). As the 2xSD of the resamples is 66.8 m, the signal-to-noise ratio is 1.24, slightly larger than the ratio 1.18 for strong sea ice forcing in CESM2-WACCM6. We also find that the minimum ensemble size needed for the 2xSD lower bound to be larger than zero is 133 (Fig. 10d), which is very close to the value of 138 from CESM2-WACCM6. This confirms that, in order to emerge beyond the level of internal variability at the 5% significance level, the stratospheric signal under strong sea ice forcing requires about 140 members in both models. As noted above,

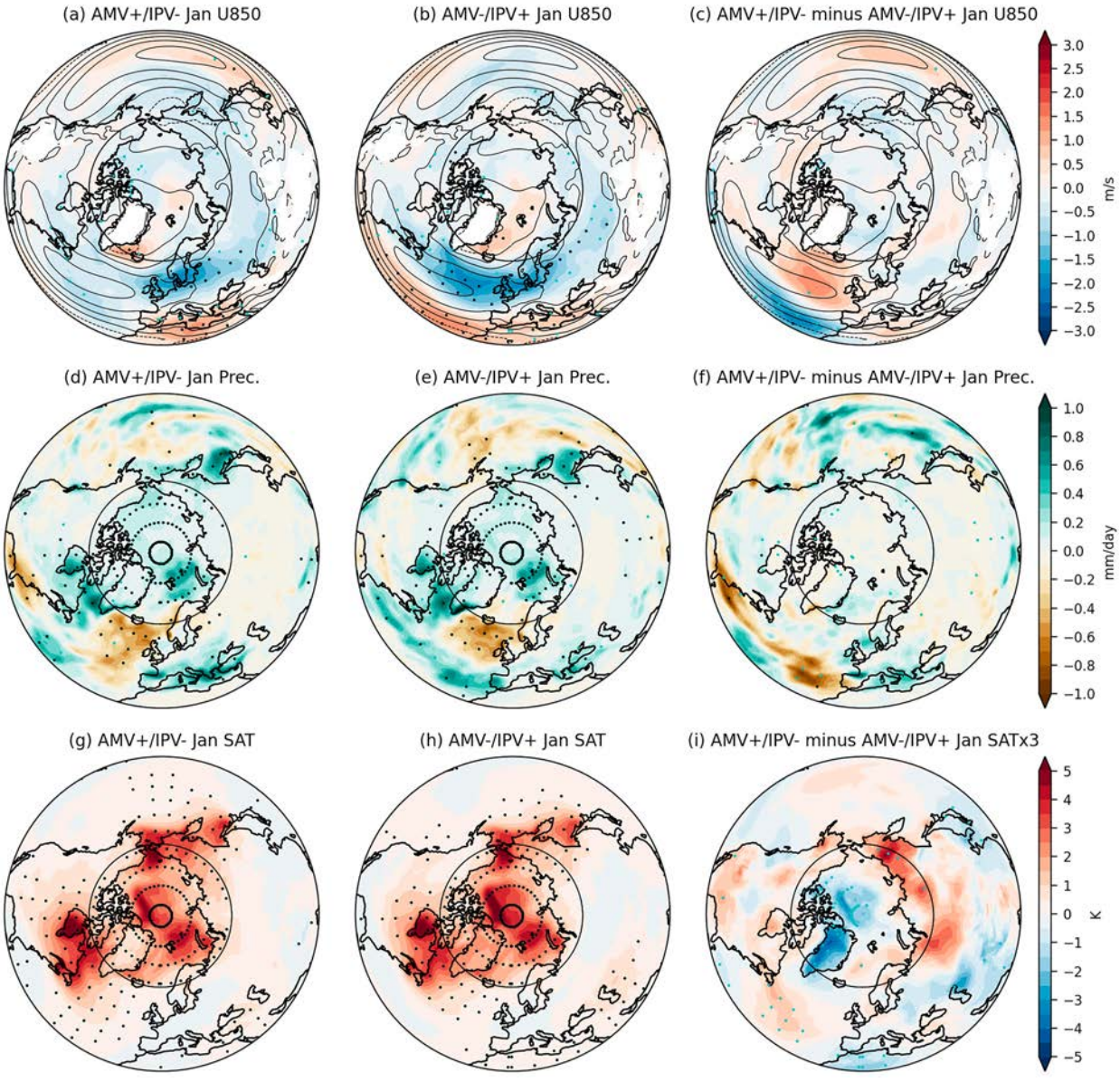

FIG. 9. January (a),(b) U850, (d),(e) total precipitation, and (g),(h) SAT responses to sea ice forcing during AMV+/IPV− and AMV−/IPV+ states, respectively. Also shown are (c) the difference between (a) and (b); (f) the difference between (d) and (e); and (i) the difference between (g) and (h). The values in (i) are multiplied by a factor of 3 for better illustration. Here, the responses to strong and weak sea ice forcings have been combined. The black dots denote the field significance, while the cyan dots denote the 5% local significance. The black contours in (a) and (b) denote the climatological mean U850 (contour interval of 4 m s^{-1}; solid contours for positive values and dashed contours for negative values).

the stratospheric response under weak sea ice forcing is small and lacks statistical significance in IPSL-CM6A-LR (the green distribution in Fig. 10c), with a signal-to-noise ratio of only 0.07.

The spatial distributions of the February Z50, Z500, and SLP responses simulated by IPSL-CM6A-LR are shown in Fig. 11. The coupled stratosphere–troposphere response occurs mostly within the Arctic Circle under strong sea ice forcing (Figs. 11a,c), different from that simulated by CESM2-WACCM6 where it occurs mainly over the North Atlantic sector (Figs. 5a,c). Moreover, the coupled response does not descend to the near surface as no statistically significant SLP responses appear (Fig. 11e). Correspondingly, the U850 and precipitation responses are not robust (Figs. 12a,c). Like CESM2-WACCM6, the SAT responses are localized to the areas of maximum sea ice loss (Fig. 12e). Under the weak SIC forcing, no clear stratosphere–troposphere coupled response occurs (Figs. 11b,d,f) and no robust near-surface climate responses exist (Figs. 12b,d,f).

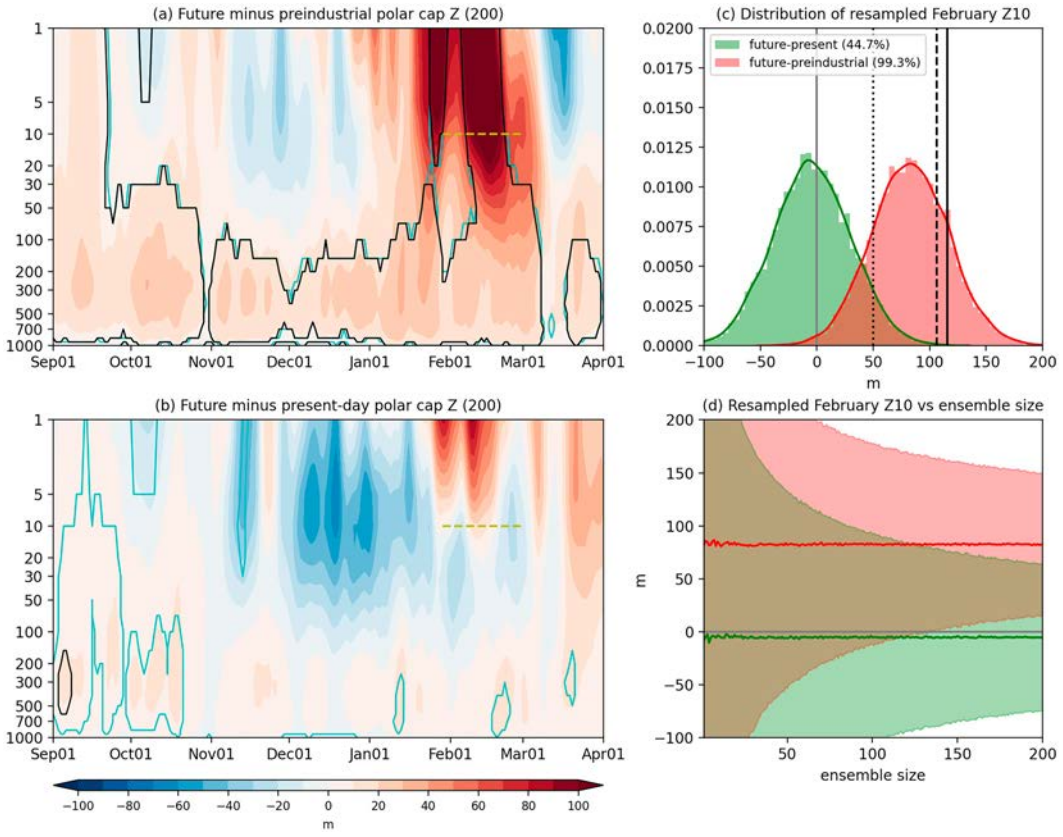

FIG. 10. As in Fig. 4, but using IPSL-CM6A-LR. Note that (c) and (d) are based on February Z10 responses [indicated by dashed yellow lines in (a) and (b), respectively].

4. Discussion

The results presented in this study support previous findings that Arctic sea ice loss can influence midlatitude surface climate via a stratospheric pathway (Jaiser et al. 2013; Cohen et al. 2014; Kim et al. 2014; Jaiser et al. 2016; Nakamura et al. 2016; Ruggieri et al. 2016). However, some aspects warrant further discussion. The first issue relates to the methodology used to constrain sea ice in coupled model experiments, as the PAMIP protocol did not require a unified approach, and different methods may produce varied results as suggested based on idealized model configurations (England et al. 2022). In our CESM2-WACCM6 simulations, we utilize a nudging technique to constrain the sea ice condition toward the PAMIP target. However, this sea ice nudging technique has been suggested to produce a spurious warming over the Northern Hemisphere in both idealized models and GCMs that may cause an overestimation of the climate responses to sea ice loss (England et al. 2022). In addition, varying sea ice thickness can contribute to recent Arctic warming (Gerdes 2006; Lang et al. 2017; Labe et al. 2018), but sea ice thickness was constrained to be 2 m in our experiments, as specified in the PAMIP protocol. It is noted that the IPSL-CM6A-LR only constrains SIC, not SIV. This could lead to a different sea ice thickness profile from that of CESM-WACMM6 and contribute to the different degrees of Arctic warming. In addition, several recent studies showed that the stratospheric polar vortex could also directly affect the Arctic sea ice, allowing for two-way interactions between the stratospheric vortex and sea ice (e.g., Smith et al. 2018; Kelleher et al. 2020; J. Zhang et al. 2022). In our simulations, as the sea ice condition is nudged, this effect cannot be included. Further modeling efforts are needed to improve our understanding of this aspect and its contribution to midlatitude circulation changes.

The next issue pertains to the influence of internal variability (i.e., the signal-to-noise ratio). In particular, Sun et al. (2022) showed that two different 100-member ensemble averages of stratospheric (10 hPa) zonal-mean zonal wind response to PAMIP sea ice forcing can be of opposite sign because the signal-to-noise ratio in their experiment was very small. In our CESM2-WACCM6 simulations with the signal-to-noise ratio of 1.18 for December Z10 in response to the strong sea ice forcing, we do not find such stark contrast between the first (dotted vertical line in Fig. 4c) and second (solid vertical line in Fig. 4c) 100-member averages of the December Z10 stratospheric response, both of which lie close to the 200-member average, and indeed within one standard deviation of the full distribution. We also calculate the middle 100-member (i.e., 51–150 members) average (dashed vertical line in Fig. 4c), and it is again close to the 200-member average. While the IPSL-CM6A-LR simulations show a wider

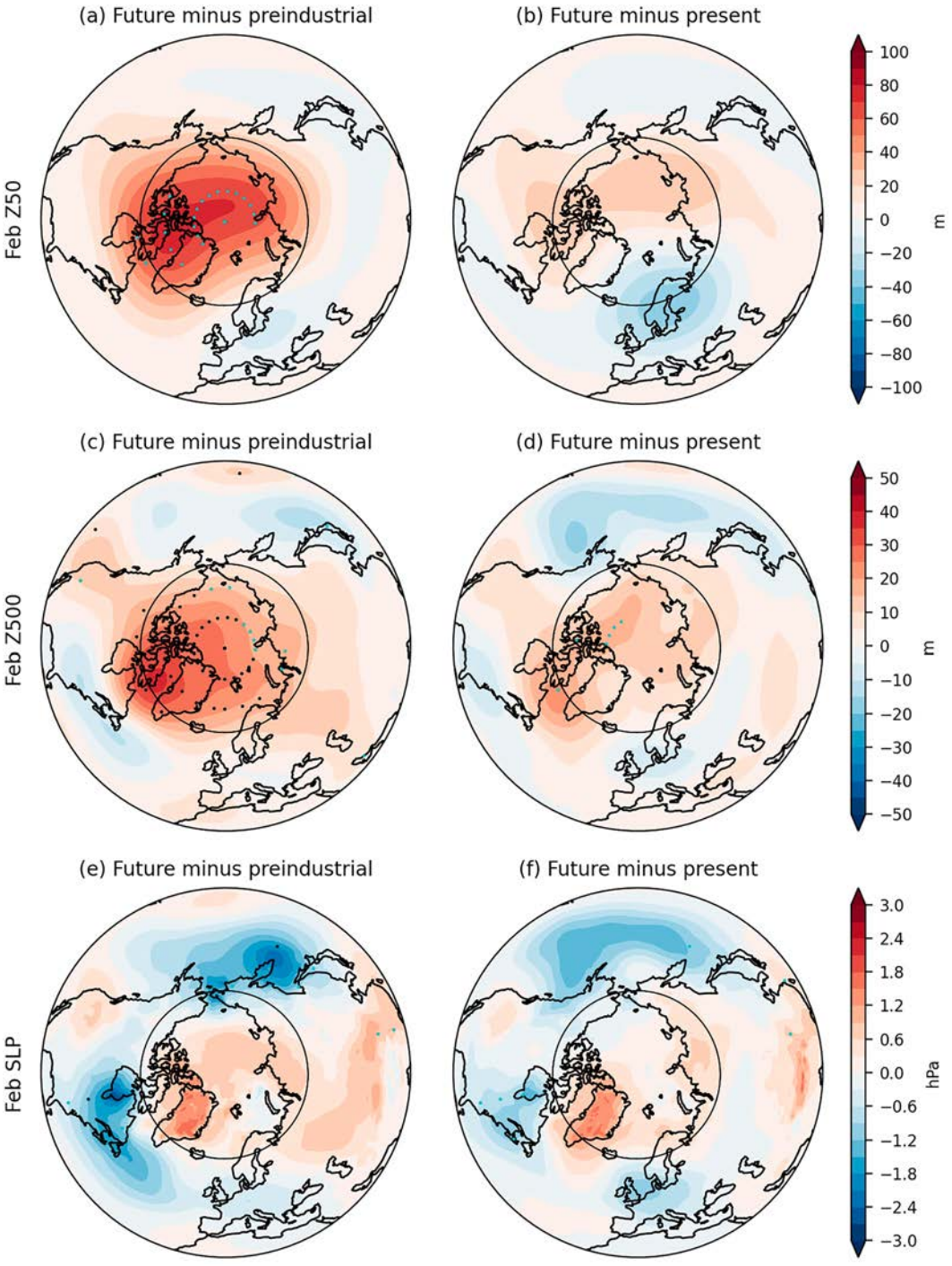

FIG. 11. As in Fig. 5, but using IPSL-CM6A-LR and for February.

range between the discrete 100-member averages of February Z10 (vertical lines in Fig. 10c), they are still not as extreme as in Sun et al. (2022), because the IPSL-CM6A-LR simulations had the signal-to-noise ratio of 1.24 for February Z10. Moreover, Sun et al. (2022) analyzed atmosphere-only simulations, which do not allow two-way coupling between the atmosphere, ocean, and sea ice. Previous studies have indicated that including atmosphere–ocean dynamical coupling can amplify the atmospheric response to Arctic sea ice loss (Deser et al. 2015, 2016) and therefore enhance the signal-to-noise ratio. Also, Sun et al. (2022) used CAM6 with low-top configuration, in which the frequency of sudden stratospheric warming events is underestimated (Ayarzagüena et al. 2020), whereas both CESM2-WACCM6 and IPSL-CM6A-LR have a high-top

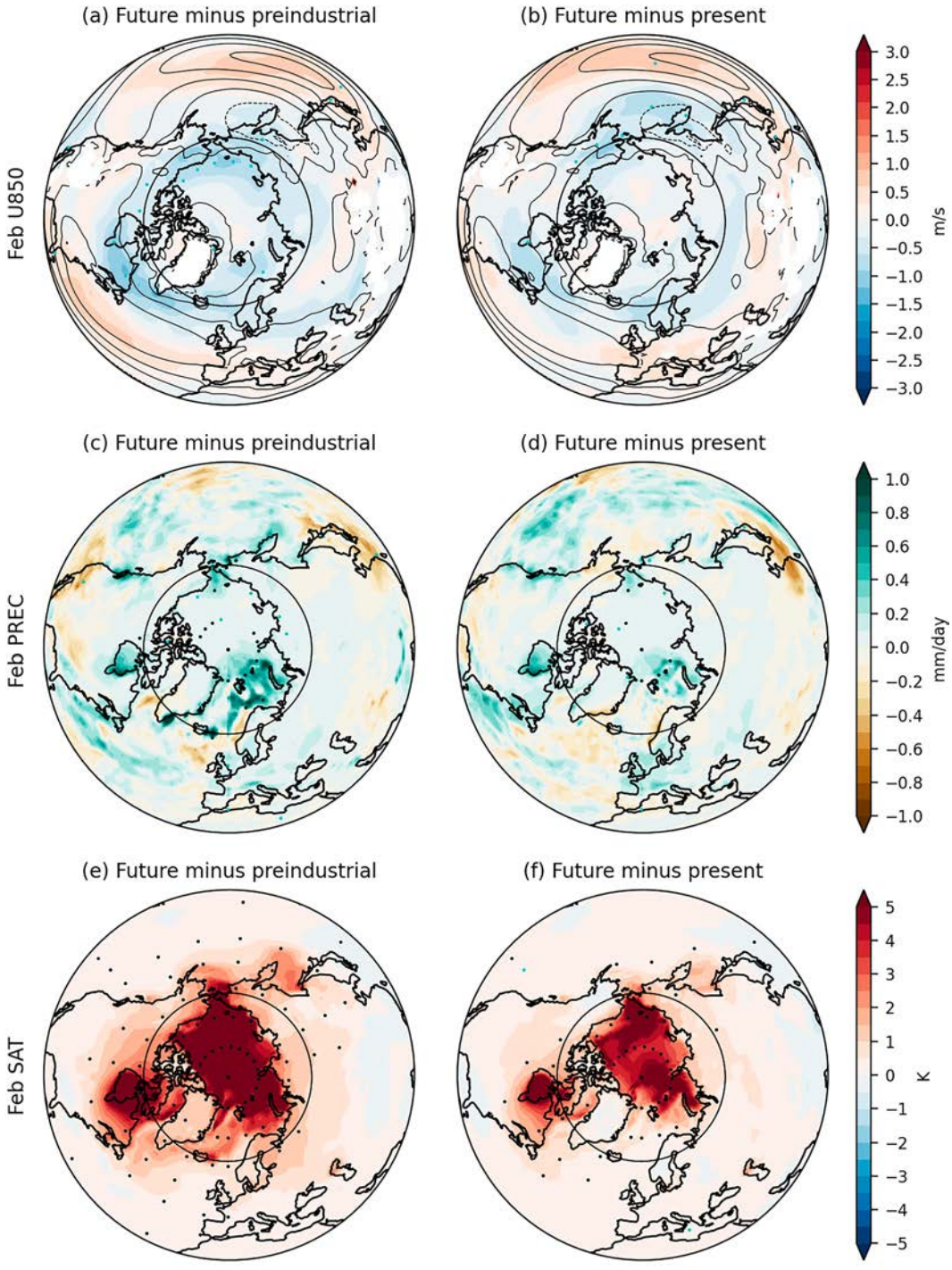

FIG. 12. As in Fig. 6, but using IPSL-CM6A-LR and for February.

configuration. In addition, Smith et al. (2022) reported that, by looking into multimodel means in December–February, weak but reduced EP fluxes appear. This is different from our single-model results in a given December or February and deserves further analysis to uncover the essential reason.

Compared with observation/reanalysis data-based studies, our modeling results show apparent discrepancies in time and space. For example, Kim et al. (2014) and Romanowsky et al. (2019) used reanalysis data to show that the largest stratospheric response occurs in January and February, later than the stratospheric response of our CESM2-WACCM6 simulations,

which already emerges in December. Also, Furtado (2019) found that blocking in the Ural Mountain and Scandinavia was a tropospheric precursor of stratospheric response. However, no such patterns present in our simulations; instead, only reduced SLP over the pan-Arctic domain emerges. Therefore, it would be important to understand why these spatiotemporal discrepancies between observations/reanalysis data and GCM simulations occur.

Last, previous modeling studies showed that an AMV+ state tends to give a negative NAO-like response pattern during boreal winter (Peings and Magnusdottir 2016; Elsbury et al. 2019; Kwon et al. 2020). Instead, comparing January–February SLP responses in our AMV+/IPV− and AMV−/IPV+ ensemble means, the former produces a less coherent negative NAO-like pattern in response to sea ice decrease than the latter (cf. Figs. 8a,b). This is likely caused by a more southerly eddy-driven jet position, which is associated with the NAO negative phase preferred by the AMV+ state, inhibiting a strong midlatitude tropospheric circulation response to the sea ice decline (Smith et al. 2017). It is also possibly due to the concurrent impacts of AMV+ and IPV−, which leads to positive and negative NAO-like patterns, respectively (Elsbury et al. 2019). Thus, the negative NAO signal from AMV+ may be somewhat offset by that from IPV− in the AMV+/IPV− case. In addition, we cannot rule out the nonlinear interplay between AMV and IPV and the associated impact on the stratospheric and tropospheric responses (e.g., Davini et al. 2015; Ruprich-Robert et al. 2017; Sun et al. 2017; Elsbury et al. 2019; Meehl et al. 2021). It is also noted that our calculation of the AMV index could introduce spurious climatic responses (Frankignoul et al. 2017; Deser and Phillips 2023). Whether or not this artificial effect can influence the atmospheric responses to Arctic sea ice loss deserves further investigation.

5. Summary

This study uses the high-top CESM2-WACCM6 coupled model, for the first time, to conduct time-slice experiments following the PAMIP protocol (Smith et al. 2019), different from previous studies that used atmosphere-only models (e.g., Xu et al. 2021; Zhang and Screen 2021; Sun et al. 2022). The sea ice conditions are constrained to preindustrial, present, and future states throughout a 14-month integration period in order to examine the large-scale circulation responses in the stratosphere and troposphere under varying strengths of Arctic sea ice loss. We consider the difference between the future and preindustrial runs as the response under strong sea ice forcing, and that between the future and present runs as the response under weak sea ice forcing. We focus on the stratospheric response and the subsequent near-surface impacts: that is, the so-called stratospheric pathway linking Arctic climate change to midlatitude impacts. As recent studies found that the recommended ensemble size in the PAMIP protocol (100 members) is too small to robustly distinguish the signal from sea ice forcing from the noise of internal variability (e.g., Labe et al. 2019; Liang et al. 2020; Peings et al. 2021; Sun et al. 2022), we have enlarged our set of simulations to 200 members. To investigate whether different background ocean states can modulate aspects of the response to Arctic sea ice loss, we initialized half of the ensemble members (i.e., 100 members) with the AMV+/IPV− state and the other half with the AMV−/IPV+ SST patterns.

Following the classic framework to analyze stratosphere–troposphere coupling (Baldwin and Dunkerton 2001), we have shown that Arctic sea ice loss produces significant precursor SLP structures during November with decreased values over the Arctic Ocean and increased values over North Atlantic and Eurasia, together with enhanced upward wave activity into the stratosphere. Via wave–mean flow interaction, the resultant wave drag weakens the stratospheric polar vortex and elevates the polar cap geopotential height in December. Then, in January–February, the perturbed stratospheric circulation gradually migrates downward to the lower troposphere with a negative NAO-like pattern and an enhanced ridge near the Ural Mountains, affecting the magnitude and location of the tropospheric eddy-driven jet and precipitation in Eurasia. The stronger the sea ice forcing, the greater the stratosphere–troposphere responses (e.g., polar cap Z and negative NAO) and the broader their spatial extents (e.g., high SLP extending into central China).

In light of the low signal-to-noise of the simulated response to Arctic sea ice loss (e.g., Labe et al. 2019; Liang et al. 2020; Peings et al. 2021; Sun et al. 2022), we use a random sampling technique to robustly quantify the effect of internal variability on the stratospheric response in December, when the response reaches its peak in our CESM2-WACCM6 simulations. We show that the ensemble-mean Z10 response is twice as large under strong sea ice forcing than weak sea ice forcing. On the other hand, the amplitude of internal variability, measured by two standard deviations of the probability density function of December polar cap Z10, is not substantially affected by the magnitude of sea ice loss: hence, the signal-to-noise ratio of the response increases by approximately a factor of 2 (1.18 vs 0.66) under strong versus weak sea ice forcing. We also find that 130–140 members are needed to distinguish the stratospheric response from the noise of internal variability with 95% confidence for strong sea ice forcing, while 200 members do not suffice for weak sea ice forcing. A similar ensemble size requirement is found for the experiments with IPSL-CM6A-LR in the strong sea ice forcing case.

To investigate whether AMV and IPV states modulate the response to sea ice loss, which is the major novelty of this study, we combine the 100 members of the weak and strong sea ice forcing cases to obtain a total of 200 members under the AMV+/IPV− and AMV−/IPV+ states. In the sense of polar-cap average, the AMV+/IPV− state favors downward migration of stratospheric responses to the near surface during late December and January, while the AMV−/IPV+ shows less coupling between the stratosphere and troposphere but stronger tropospheric responses. The surface impacts in January modulated by AMV and IPV states are apparent in the North Atlantic sector, manifested as the negative NAO-like circulation pattern in the middle and lower troposphere, precipitation decrease, and weakened or shifting of the Atlantic

jet stream. The AMV+/IPV− state tends to shift the weakened jet stream toward northern Europe. On the other hand, varying AMV and IPV states do not seem to strongly modulate the near-surface temperature response to sea ice loss. It is noted that more ensemble members are appreciated for the weak and strong cases to confirm that the above findings, based on the mixture of the two, are robust.

We also considered parallel sets of PAMIP experiments with the IPSL-CM6A-LR coupled model to investigate if stratosphere–troposphere coupling forced by Arctic sea ice loss is model dependent. The maximum stratospheric response simulated by IPSL-CM6A-LR occurs in February instead of December as in CESM2-WACCM6. The stratospheric responses with IPSL-CM6A-LR only descend to the middle troposphere, but not to the near surface, distinct from stronger stratosphere and near-surface coupling simulated by CESM2-WACCM6. Model dependence requires further studies, as the timing of the strongest stratospheric response and the extent of stratosphere–troposphere coupling are different in the two models.

Taken together, our findings support the notion that Arctic sea ice loss is capable of influencing midlatitude climate via a stratospheric pathway on seasonal time scales, although the simulated circulation responses have a relatively low signal-to-noise ratio and require strong sea ice forcing (and large ensemble sizes) to be detectable. Our findings further highlight that modulations by the background oceanic mean state and model dependence need to be taken into account.

Acknowledgments. We thank two anonymous reviewers and the editor for constructive comments and suggestions to improve the quality of this manuscript. We acknowledge support by the BlueAction Project (the European Union's Horizon 2020 research and innovation programme, #727852, http://www.blue-action.eu/index.php?id53498). The WHOI group was supported by the U.S. National Science Foundation (NSF) Office of Polar Programs Grants 1736738/1737377 and 2106190/2106228. L. Sun is supported by the National Science Foundation (AGS-2300038). Y.-C. Liang was supported by the grants of the National Science and Technology Council (MOST 110-2111-M-002-019-MY2, 111-2628-M-002-011, and 112-2628-M-002-009) to National Taiwan University. NCAR was sponsored by the National Science Foundation. We would like to acknowledge the use of computational resources (https://doi.org/10.5065/D6RX99HX) at the NCAR–Wyoming Supercomputing Center provided by the National Science Foundation and the State of Wyoming and supported by NCAR's Computational and Information Systems Laboratory. For IPSL-CM6A-LR simulations, this work was granted access to the HPC resources of TGCC under the allocations A7-017403 and A11-017403 made by GENCI. The details of IPSL-CM6A-LR can be found in https://cmc.ipsl.fr.

Data availability statement. The PAMIP data with CESM2-WACCM6 and IPSL-CM6A-LR can be obtained on the Earth System Grid Federation website (https://doi.org/10.22033/ESGF/CMIP6.2197) or upon request to the corresponding author.

REFERENCES

Andrews, D. G., J. R. Holton, and C. B. Leovy, 1987: *Middle Atmosphere Dynamics.* Academic Press, 489 pp.

Audette, A., and Coauthors, 2021: Opposite responses of the dry and moist eddy heat transport into the Arctic in the PAMIP experiments. *Geophys. Res. Lett.*, **48**, e2020GL089990, https://doi.org/10.1029/2020GL0899900.

Ayarzagüena, B., and Coauthors, 2020: Uncertainty in the response of sudden stratospheric warmings and stratosphere-troposphere coupling to quadrupled CO_2 concentrations in CMIP6 models. *J. Geophys. Res. Atmos.*, **125**, e2019JD032345, https://doi.org/10.1029/2019JD032345.

Baldwin, M. P., and T. J. Dunkerton, 2001: Stratospheric harbingers of anomalous weather regimes. *Science*, **294**, 581–584, https://doi.org/10.1126/science.1063315.

——, and Coauthors, 2021: Sudden stratospheric warmings. *Rev. Geophys.*, **59**, e2020RG000708, https://doi.org/10.1029/2020RG000708.

Barnes, E. A., 2013: Revisiting the evidence linking Arctic amplification to extreme weather in midlatitudes. *Geophys. Res. Lett.*, **40**, 4734–4739, https://doi.org/10.1002/grl.50880.

——, and J. A. Screen, 2015: The impact of Arctic warming on the midlatitude jet-stream: Can it? Has it? Will it? *Wiley Interdiscip. Rev.: Climate Change*, **6**, 277–286, https://doi.org/10.1002/wcc.337.

Blackport, R., and J. A. Screen, 2019: Influence of Arctic sea ice loss in autumn compared to that in winter on the atmospheric circulation. *Geophys. Res. Lett.*, **46**, 2213–2221, https://doi.org/10.1029/2018GL081469.

——, and ——, 2020a: Weakened evidence for mid-latitude impacts of Arctic warming. *Nat. Climate Change*, **10**, 1065–1066, https://doi.org/10.1038/s41558-020-00954-y.

——, and ——, 2020b: Insignificant effect of Arctic amplification on the amplitude of midlatitude atmospheric waves. *Sci. Adv.*, **6**, eaay2880, https://doi.org/10.1126/sciadv.aay2880.

——, ——, K. van der Wiel, and R. Bintanja, 2019: Minimal influence of reduced Arctic sea ice on coincident cold winters in mid-latitudes. *Nat. Climate Change*, **9**, 697–704, https://doi.org/10.1038/s41558-019-0551-4.

Boucher, O., and Coauthors, 2020: Presentation and evaluation of the IPSL-CM6A-LR climate model. *J. Adv. Model. Earth Syst.*, **12**, e2019MS002010, https://doi.org/10.1029/2019MS002010.

Cai, D., M. Dameris, H. Garny, and T. Runde, 2012: Implications of all season Arctic sea-ice anomalies on the stratosphere. *Atmos. Chem. Phys.*, **12**, 11 819–11 831, https://doi.org/10.5194/acp-12-11819-2012.

Cassano, E. N., J. J. Cassano, M. E. Higgins, and M. C. Serreze, 2014: Atmospheric impacts of an Arctic sea ice minimum as seen in the Community Atmosphere Model. *Int. J. Climatol.*, **34**, 766–779, https://doi.org/10.1002/joc.3723.

Cavalieri, D. J., and C. L. Parkinson, 2012: Arctic sea ice variability and trends, 1979–2010. *Cryosphere*, **6**, 881–889, https://doi.org/10.5194/tc-6-881-2012.

Chen, H. W., F. Zhang, and R. B. Alley, 2016: The robustness of midlatitude weather pattern changes due to Arctic sea ice loss. *J. Climate*, **29**, 7831–7849, https://doi.org/10.1175/JCLI-D-16-0167.1.

Chen, Y., D. Luo, and L. Zhong, 2021: North Atlantic multidecadal footprint of the recent winter warm Arctic–cold Siberia pattern. *Climate Dyn.*, **57**, 121–139, https://doi.org/10.1007/s00382-021-05698-9.

Chylek, P., C. Folland, J. D. Klett, M. Wang, N. Hengartner, G. Lesins, and M. K. Dubey, 2022: Annual mean Arctic amplification 1970–2020: Observed and simulated by CMIP6 climate models. *Geophys. Res. Lett.*, **49**, e2022GL099371, https://doi.org/10.1029/2022GL099371.

Cohen, J., and Coauthors, 2014: Recent Arctic amplification and extreme mid-latitude weather. *Nat. Geosci.*, **7**, 627–637, https://doi.org/10.1038/ngeo2234.

——, K. Pfeiffer, and J. A. Francis, 2018: Warm Arctic episodes linked with increased frequency of extreme winter weather in the United States. *Nat. Commun.*, **9**, 869, https://doi.org/10.1038/s41467-018-02992-9.

——, and Coauthors, 2020: Divergent consensuses on Arctic amplification influence on midlatitude severe winter weather. *Nat. Climate Change*, **10**, 20–29, https://doi.org/10.1038/s41558-019-0662-y.

Comiso, J. C., C. L. Parkinson, R. Gersten, and L. Stock, 2008: Accelerated decline in the Arctic sea ice cover. *Geophys. Res. Lett.*, **35**, L01703, https://doi.org/10.1029/2007GL031972.

Coumou, D., G. D. Capua, S. Vavrus, L. Wang, and S. Wang, 2018: The influence of Arctic amplification on mid-latitude summer circulation. *Nat. Commun.*, **9**, 2959, https://doi.org/10.1038/s41467-018-05256-8.

Dai, A., and M. Song, 2020: Little influence of Arctic amplification on mid-latitude climate. *Nat. Climate Change*, **10**, 231–237, https://doi.org/10.1038/s41558-020-0694-3.

Danabasoglu, G., and Coauthors, 2020: The Community Earth System Model version 2 (CESM2). *J. Adv. Model. Earth Syst.*, **12**, e2019MS001916, https://doi.org/10.1029/2019MS001916.

Davini, P., J. von Hardenberg, and S. Corti, 2015: Tropical origin for the impacts of the Atlantic multidecadal variability on the Euro-Atlantic climate. *Environ. Res. Lett.*, **10**, 094010, https://doi.org/10.1088/1748-9326/10/9/094010.

Deser, C. and A. S. Phillips, 2023: Spurious Indo-Pacific connections to internal Atlantic Multidecadal Variability introduced by the global temperature residual method. *Geophys. Res. Lett.*, **50**, e2022GL100574, https://doi.org/10.1029/2022GL100574.

——, G. Magnusdottir, R. Saravanan, and A. Phillips, 2004: The effects of North Atlantic SST and sea-ice anomalies on the winter circulation in CCM3. Part II: Direct and indirect components of the response. *J. Climate*, **17**, 877–889, https://doi.org/10.1175/1520-0442(2004)017<0877:TEONAS>2.0.CO;2.

——, A. S. Phillips, and M. A. Alexander, 2010a: Twentieth century tropical sea surface temperature trends revisited. *Geophys. Res. Lett.*, **37**, L10701, https://doi.org/10.1029/2010GL043321.

——, R. A. Tomas, M. A. Alexander, and D. Lawrence, 2010b: The seasonal atmospheric response to projected Arctic sea ice loss in the late twenty-first century. *J. Climate*, **23**, 333–351, https://doi.org/10.1175/2009JCLI3053.1.

——, ——, and L. Sun, 2015: The role of ocean–atmosphere coupling in the zonal-mean atmospheric response to Arctic sea ice loss. *J. Climate*, **28**, 2168–2186, https://doi.org/10.1175/JCLI-D-14-00325.1.

——, L. Sun, R. A. Tomas, and J. Screen, 2016: Does ocean coupling matter for the northern extratropical response to projected Arctic sea ice loss? *Geophys. Res. Lett.*, **43**, 2149–2157, https://doi.org/10.1002/2016GL067792.

——, and Coauthors, 2020: Insights from Earth system model initial-condition large ensembles and future prospects. *Nat. Climate Change*, **10**, 277–286, https://doi.org/10.1038/s41558-020-0731-2.

Domeisen, D. I. V., and A. H. Butler, 2020: Stratospheric drivers of extreme events at the Earth's surface. *Commun. Earth Environ.*, **1**, 59, https://doi.org/10.1038/s43247-020-00060-z.

——, and Coauthors, 2020: The role of the stratosphere in subseasonal to seasonal prediction: 2. Predictability arising from stratosphere-troposphere coupling. *J. Geophys. Res. Atmos.*, **125**, e2019JD030923, https://doi.org/10.1029/2019JD030923.

Edmon, H. J., Jr., B. J. Hoskins, and M. E. McIntyre, 1980: Eliassen-Palm cross sections for the troposphere. *J. Atmos. Sci.*, **37**, 2600–2616, https://doi.org/10.1175/1520-0469(1980)037<2600:EPCSFT>2.0.CO;2.

Elsbury, D., Y. Peings, D. Saint-Martin, H. Douville, and G. Magnusdottir, 2019: The atmospheric response to positive IPV, positive AMV, and their combination in boreal winter. *J. Climate*, **32**, 4193–4213, https://doi.org/10.1175/JCLI-D-18-0422.1.

Enfield, D. B., A. M. Mestas-Nuñez, and P. J. Trimble, 2001: The Atlantic multidecadal oscillation and its relationship to rainfall and river flows in the continental U.S. *Geophys. Res. Lett.*, **28**, 2077–2080, https://doi.org/10.1029/2000GL012745.

England, M., L. Polvani, and L. Sun, 2018: Contrasting the Antarctic and Arctic atmospheric responses to projected sea ice loss in the late twenty-first century. *J. Climate*, **31**, 6353–6370, https://doi.org/10.1175/JCLI-D-17-0666.1.

——, I. Eisenman, N. J. Lutsko, and T. J. W. Wagner, 2021: The recent emergence of Arctic amplification. *Geophys. Res. Lett.*, **48**, e2021GL094086, https://doi.org/10.1029/2021GL094086.

——, ——, and T. J. W. Wagner, 2022: Spurious climate impacts in coupled sea ice loss simulations. *J. Climate*, **35**, 7401–7411, https://doi.org/10.1175/JCLI-D-21-0647.1.

Eyring, V., S. Bony, G. A. Meehl, C. A. Senior, B. Stevens, R. J. Stouffer, and K. E. Taylor, 2016: Overview of the Coupled Model Intercomparison Project Phase 6 (CMIP6) experimental design and organization. *Geosci. Model Dev.*, **9**, 1937–1958, https://doi.org/10.5194/gmd-9-1937-2016.

Fetterer, F., K. Knowles, W. N. Meier, M. Savoie, and A. K. Windnagel, 2017: Sea Ice Index, version 3. National Snow and Ice Data Center, accessed 16 July 2021, https://doi.org/10.7265/N5K072F8.

Francis, J. A., and S. J. Vavrus, 2012: Evidence linking Arctic amplification to extreme weather in mid-latitudes. *Geophys. Res. Lett.*, **39**, L06801, https://doi.org/10.1029/2012GL051000.

——, and ——, 2015: Evidence for a wavier jet stream in response to rapid Arctic warming. *Environ. Res. Lett.*, **10**, 014005, https://doi.org/10.1088/1748-9326/10/1/014005.

——, N. Skific, and S. J. Vavrus, 2018: North American weather regimes are becoming more persistent: Is Arctic amplification a factor? *Geophys. Res. Lett.*, **45**, 11 414–11 422, https://doi.org/10.1029/2018GL080252.

Frankignoul, C., G. Gastineau, and Y.-O. Kwon, 2017: Estimation of the SST response to anthropogenic and external forcing, and its impact on the Atlantic multidecadal oscillation and the Pacific decadal oscillation. *J. Climate*, **30**, 9871–9895, https://doi.org/10.1175/JCLI-D-17-0009.1.

Furtado, J. C., 2019: Links between autumn snow cover and sea ice extent and Northern Hemisphere wintertime climate variability. *U.S. CLIVAR Variations*, Spring 2019, US CLIVAR Project Office, Washington, D.C., 12–19, https://usclivar.org/newsletters.

Gerdes, R., 2006: Atmospheric response to changes in Arctic sea ice thickness. *Geophys. Res. Lett.*, **33**, L18709, https://doi.org/10.1029/2006GL027146.

Gettelman, A., and Coauthors, 2019: The Whole Atmosphere Community Climate Model version 6 (WACCM6). *J.*

Geophys. Res. Atmos., **124**, 12 380–12 403, https://doi.org/10.1029/2019JD030943.

Goosse, H., and Coauthors, 2018: Quantifying climate feedbacks in polar regions. *Nat. Commun.*, **9**, 1919, https://doi.org/10.1038/s41467-018-04173-0.

Grebmeier, J. M., 2012: Shifting patterns of life in the Pacific Arctic and sub-Arctic seas. *Annu. Rev. Mar. Sci.*, **4**, 63–78, https://doi.org/10.1146/annurev-marine-120710-100926.

Hahn, L. C., K. C. Armour, M. D. Zelinka, C. M. Bitz, and A. Donohoe, 2021: Contributions to polar amplification in CMIP5 and CMIP6 models. *Front. Earth Sci.*, **9**, 710036, https://doi.org/10.3389/feart.2021.710036.

Harvey, B. J., L. C. Shaffrey, and T. J. Woollings, 2014: Equator-to-pole temperature differences and the extra-tropical storm track responses of the CMIP5 climate models. *Climate Dyn.*, **43**, 1171–1182, https://doi.org/10.1007/s00382-013-1883-9.

Hausfather, Z., 2020: Analysis: When might the world exceed 1.5°C and 2°C of global warming? World Economy Forum, accessed 2 June 2021, https://www.weforum.org/agenda/2020/12/analysis-world-paris-agreement-climate-targets-change-emissions-global-warming/.

Haustein, K., M. R. Allen, P. M. Forster, F. E. L. Otto, D. M. Mitchell, H. D. Matthews, and D. J. Frame, 2017: A real-time global warming index. *Sci. Rep.*, **7**, 15417, https://doi.org/10.1038/s41598-017-14828-5.

Henley, B. J., J. Gergis, D. J. Karoly, S. Power, J. Kennedy, and C. K. Folland, 2015: A tripole index for the interdecadal Pacific oscillation. *Climate Dyn.*, **45**, 3077–3090, https://doi.org/10.1007/s00382-015-2525-1.

Holland, M. M., and C. M. Bitz, 2003: Polar amplification of climate change in coupled models. *Climate Dyn.*, **21**, 221–232, https://doi.org/10.1007/s00382-003-0332-6.

Hourdin, F., and Coauthors, 2020: LMDZ6A: The atmospheric component of the IPSL climate model with improved and better tuned physics. *J. Adv. Model. Earth Syst.*, **12**, e2019MS001892, https://doi.org/10.1029/2019MS001892.

Hunke, E. C., W. H. Lipscomb, A. K. Turner, N. Jeffery, and S. Elliott, 2015: CICE: The Los Alamos Sea Ice Model documentation and software user's manual, version 5.1. Tech. Rep. LA-CC-06-012, 116 pp.

Hurrell, J. W., 1995: Decadal trends in the North Atlantic Oscillation: Regional temperatures and precipitation. *Science*, **269**, 676–679, https://doi.org/10.1126/science.269.5224.676.

——, Y. Kushnir, G. Ottersen, and M. Visbeck, 2003: An overview of the North Atlantic Oscillation. *The North Atlantic Oscillation: Climatic Significance and Environmental Impact*, *Geophys. Monogr.*, Vol. 134, Amer. Geophys. Union, 1–35, https://doi.org/10.1029/GM134.

IPCC, 2019: *The Ocean and Cryosphere in a Changing Climate: Special Report on the Ocean and Cryosphere in a Changing Climate*. Cambridge University Press, 755 pp., https://doi.org/10.1017/9781009157964.

——, 2021: *Climate Change 2021: The Physical Science Basis*. Cambridge University Press, 2392 pp., https://doi.org/10.1017/9781009157896.

Jaiser, R., K. Dethloff, and D. Handorf, 2013: Stratospheric response to Arctic sea ice retreat and associated planetary wave propagation changes. *Tellus*, **65A**, 19375, https://doi.org/10.3402/tellusa.v65i0.19375.

——, T. Nakamura, D. Handorf, K. Dethloff, J. Ukita, and K. Yamazaki, 2016: Atmospheric winter response to Arctic sea ice changes in reanalysis data and model simulations. *J. Geophys. Res. Atmos.*, **121**, 7564–7577, https://doi.org/10.1002/2015JD024679.

Jung, T., and Coauthors, 2016: Advancing polar prediction capabilities on daily to seasonal time scales. *Bull. Amer. Meteor. Soc.*, **97**, 1631–1647, https://doi.org/10.1175/BAMS-D-14-00246.1.

Kay, J. E., and Coauthors, 2015: The Community Earth System Model (CESM) large ensemble project: A community resource for studying climate change in the presence of internal climate variability. *Bull. Amer. Meteor. Soc.*, **96**, 1333–1349, https://doi.org/10.1175/BAMS-D-13-00255.1.

Kelleher, M. E., B. Ayarzagüena, and J. A. Screen, 2020: Interseasonal connections between the timing of the stratospheric final warming and Arctic sea ice. *J. Climate*, **33**, 3079–3092, https://doi.org/10.1175/JCLI-D-19-0064.1.

Kerr, R. A., 2000: A North Atlantic climate pacemaker for the centuries. *Science*, **288**, 1984–1985, https://doi.org/10.1126/science.288.5473.1984.

Kidston, J., A. A. Scaife, S. C. Hardiman, D. M. Mitchell, N. Butchart, M. P. Baldwin, and L. J. Gray, 2015: Stratospheric influence on tropospheric jet streams, storm tracks and surface weather. *Nat. Geosci.*, **8**, 433–440, https://doi.org/10.1038/ngeo2424.

Kim, B.-M., S.-W. Son, S.-K. Min, J.-H. Jeong, S.-J. Kim, X. Zhang, T. Shim, and J.-H. Yoon, 2014: Weakening of the stratospheric polar vortex by Arctic sea-ice loss. *Nat. Commun.*, **5**, 4646, https://doi.org/10.1038/ncomms5646.

Knight, J. R., R. J. Allan, C. K. Folland, M. Vellinga, and M. E. Mann, 2005: A signature of persistent natural thermohaline circulation cycles in observed climate. *Geophys. Res. Lett.*, **32**, L20708, https://doi.org/10.1029/2005GL024233.

Kren, A. C., D. R. Marsh, A. K. Smith, and P. Pilewskie, 2016: Wintertime Northern Hemisphere response in the stratosphere to the Pacific decadal oscillation using the Whole Atmosphere Community Climate Model. *J. Climate*, **29**, 1031–1049, https://doi.org/10.1175/JCLI-D-15-0176.1.

Kretschmer, M., D. Coumou, J. F. Donges, and J. Runge, 2016: Using causal effect networks to analyze different Arctic drivers of midlatitude winter circulation. *J. Climate*, **29**, 4069–4081, https://doi.org/10.1175/JCLI-D-15-0654.1.

Krinner, G., and Coauthors, 2005: A dynamic global vegetation model for studies of the coupled atmosphere-biosphere system. *Global Biogeochem. Cycles*, **19**, GB1015, https://doi.org/10.1029/2003GB002199.

Kwok, R., 2018: Arctic sea ice thickness, volume, and multiyear ice coverage: Losses and coupled variability (1958–2018). *Environ. Res. Lett.*, **13**, 105005, https://doi.org/10.1088/1748-9326/aae3ec.

Kwon, Y.-O., H. Seo, C. C. Ummenhofer, and T. M. Joyce, 2020: Impact of multidecadal variability in Atlantic SST on winter atmospheric blocking. *J. Climate*, **33**, 867–892, https://doi.org/10.1175/JCLI-D-19-0324.1.

Labe, Z., Y. Peings, and G. Magnusdottir, 2018: Contributions of ice thickness to the atmospheric response from projected Arctic sea ice loss. *Geophys. Res. Lett.*, **45**, 5635–5642, https://doi.org/10.1029/2018GL078158.

——, ——, and ——, 2019: The effect of QBO phase on the atmospheric response to projected Arctic sea ice loss in early winter. *Geophys. Res. Lett.*, **46**, 7663–7671, https://doi.org/10.1029/2019GL083095.

Lang, A., S. Yang, and E. Kaas, 2017: Sea ice thickness and recent Arctic warming. *Geophys. Res. Lett.*, **44**, 409–418, https://doi.org/10.1002/2016GL071274.

Lawrence, D. M., and Coauthors, 2019: The Community Land Model version 5: Description of new features, benchmarking, and impact of forcing uncertainty. *J. Adv. Model. Earth Syst.*, **11**, 4245–4287, https://doi.org/10.1029/2018MS001583.

Li, F., Y. J. Orsolini, H. Wang, Y. Gao, and S. He, 2018: Atlantic multidecadal oscillation modulates the impacts of Arctic sea ice decline. *Geophys. Res. Lett.*, **45**, 2497–2506, https://doi.org/10.1002/2017GL076210.

Li, H., M. S. Wigmosta, H. Wu, M. Huang, Y. Ke, A. M. Coleman, and L. R. Leung, 2013: A physically based runoff routing model for land surface and Earth system models. *J. Hydrometeor.*, **14**, 808–828, https://doi.org/10.1175/JHM-D-12-015.1.

Liang, Y.-C., and Coauthors, 2020: Quantification of the Arctic sea ice–driven atmospheric circulation variability in coordinated large ensemble simulations. *Geophys. Res. Lett.*, **47**, e2019GL085397, https://doi.org/10.1029/2019GL085397.

——, Y.-O. Kwon, and C. Frankignoul, 2021a: Autumn Arctic Pacific sea-ice dipole as a source of predictability for subsequent spring Barents sea-ice condition. *J. Climate*, **34**, 787–804, https://doi.org/10.1175/JCLI-D-20-0172.1.

——, and Coauthors, 2021b: Impacts of Arctic sea ice on cold season atmospheric variability and trends estimated from observations and a multi-model large ensemble. *J. Climate*, **34**, 8419–8443, https://doi.org/10.1175/JCLI-D-20-0578.1.

——, L. M. Polvani, M. Previdi, K. L. Smith, M. R. England, and G. Chiodo, 2022a: Stronger Arctic amplification from ozone-depleting substances than from carbon dioxide. *Environ. Res. Lett.*, **17**, 024010, https://doi.org/10.1088/1748-9326/ac4a31.

——, ——, and I. Mitevski, 2022b: Arctic amplification, and its seasonal migration, over a wide range of abrupt CO_2 forcing. *npj Climate Atmos. Sci.*, **5**, 14, https://doi.org/10.1038/s41612-022-00228-8.

Lin, S.-J., and R. B. Rood, 1997: An explicit flux-form semi-Lagrangian shallow water model on the sphere. *Quart. J. Roy. Meteor. Soc.*, **123**, 2477–2498, https://doi.org/10.1002/qj.49712354416.

Lindsay, R., and A. Schweiger, 2015: Arctic sea ice thickness loss determined using subsurface, aircraft, and satellite observations. *Cryosphere*, **9**, 269–283, https://doi.org/10.5194/tc-9-269-2015.

Lipscomb, W. H., and Coauthors, 2019: Description and evaluation of the Community Ice Sheet Model (CISM) v2.1. *Geosci. Model Dev.*, **12**, 387–424, https://doi.org/10.5194/gmd-12-387-2019.

Livezey, R. E., and W. Y. Chen, 1983: Statistical field significance and its determination by Monte Carlo techniques. *Mon. Wea. Rev.*, **111**, 46–59, https://doi.org/10.1175/1520-0493(1983)111%3C0046:SFSAID%3E2.0.CO;2.

Luo, B., D. Luo, A. Dai, I. Simmonds, and L. Wu, 2022: Decadal variability of winter warm Arctic-cold Eurasia dipole patterns modulated by Pacific decadal oscillation and Atlantic multidecadal oscillation. *Earth's Future*, **10**, e2021EF002351, https://doi.org/10.1029/2021EF002351.

Madec, G., R. Bourdallé-Badie, P. A. Bouttier, C. Bricaud, D. Bruciaferri, D. Calvert, and M. Vancoppenolle, 2017: NEMO ocean engine, version v3.6. Notes du Pôle de modélisation de l'Institut Pierre-Simon Laplace (IPSL) 27, 373 pp., https://doi.org/10.5281/zenodo.1472492.

Manabe, S., and R. T. Wetherald, 1975: The effects of doubling the CO_2 concentration on the climate of a general circulation model. *J. Atmos. Sci.*, **32**, 3–15, https://doi.org/10.1175/1520-0469(1975)032<0003:TEODTC>2.0.CO;2.

Markus, T., J. C. Stroeve, and J. Miller, 2009: Recent changes in Arctic sea ice melt onset, freezeup, and melt season length. *J. Geophys. Res.*, **114**, C12024, https://doi.org/10.1029/2009JC005436.

Meehl, G. A., and Coauthors, 2021: Atlantic and Pacific tropics connected by mutually interactive decadal-timescale processes. *Nat. Geosci.*, **14**, 36–42, https://doi.org/10.1038/s41561-020-00669-x.

Mori, M., M. Watanabe, H. Shiogama, J. Inoue, and M. Kimoto, 2014: Robust Arctic sea-ice influence on the frequent Eurasian cold winters in past decades. *Nat. Geosci.*, **7**, 869–873, https://doi.org/10.1038/ngeo2277.

——, Y. Kosaka, M. Watanabe, H. Nakamura, and M. Kimoto, 2019a: A reconciled estimate of the influence of Arctic sea-ice loss on recent Eurasian cooling. *Nat. Climate Change*, **9**, 123–129, https://doi.org/10.1038/s41558-018-0379-3.

——, ——, ——, B. Taguchi, H. Nakamura, and M. Kimoto, 2019b: Reply to: Is sea-ice-driven Eurasian cooling too weak in models? *Nat. Climate Change*, **9**, 937–939, https://doi.org/10.1038/s41558-019-0636-0.

Mudelsee, M., 2010: *Climate Time Series Analysis: Classical Statistical and Bootstrap Methods*. 1st ed. Springer, 474 pp.

Nakamura, T., K. Yamazaki, K. Iwamoto, M. Honda, Y. Miyoshi, Y. Ogawa, Y. Tomikawa, and J. Ukita, 2016: The stratospheric pathway for Arctic impacts on midlatitude climate. *Geophys. Res. Lett.*, **43**, 3494–3501, https://doi.org/10.1002/2016GL068330.

Nishii, K., H. Nakamura, and Y. J. Orsolini, 2010: Cooling of the wintertime Arctic stratosphere induced by the western Pacific teleconnection pattern. *Geophys. Res. Lett.*, **37**, L13805, https://doi.org/10.1029/2010GL043551.

Notz, D., and Coauthors, 2020: Arctic sea ice in CMIP6. *Geophys. Res. Lett.*, **47**, e2019GL086749, https://doi.org/10.1029/2019GL086749.

Oehrlein, J., G. Chiodo, and L. M. Polvani, 2019: Separating and quantifying the distinct impacts of El Niño and sudden stratospheric warmings on North Atlantic and Eurasian wintertime climate. *Atmos. Sci. Lett.*, **20**, e923, https://doi.org/10.1002/asl.923.

Omrani, N.-E., N. S. Keenlyside, J. Bader, and E. Manzini, 2014: Stratosphere key for wintertime atmospheric response to warm Atlantic decadal conditions. *Climate Dyn.*, **42**, 649–663, https://doi.org/10.1007/s00382-013-1860-3.

——, N. Keenlyside, K. Matthes, L. Boljka, D. Zanchettin, J. H. Jungclaus, and S. W. Lubis, 2022: Coupled stratosphere-troposphere-Atlantic multidecadal oscillation and its importance for near-future climate projection. *npj Climate Atmos. Sci.*, **5**, 59, https://doi.org/10.1038/s41612-022-00275-1.

Osborne, J. M., J. A. Screen, and M. Collins, 2017: Ocean–atmosphere state dependence of the atmospheric response to Arctic sea ice loss. *J. Climate*, **30**, 1537–1552, https://doi.org/10.1175/JCLI-D-16-0531.1.

Overland, J., J. A. Francis, R. Hall, E. Hanna, S.-J. Kim, and T. Vihma, 2015: The melting Arctic and midlatitude weather patterns: Are they connected? *J. Climate*, **28**, 7917–7932, https://doi.org/10.1175/JCLI-D-14-00822.1.

——, and Coauthors, 2016: Nonlinear response of mid-latitude weather to the changing Arctic. *Nat. Climate Change*, **6**, 992–999, https://doi.org/10.1038/nclimate3121.

Park, H.-S., S.-J. Kim, A. L. Stewart, S.-W. Son, and K.-H. Seo, 2019: Mid-Holocene Northern Hemisphere warming driven by Arctic amplification. *Sci. Adv.*, **5**, eaax8203, https://doi.org/10.1126/sciadv.aax8203.

Pedregosa, F., and Coauthors, 2011: Scikit-learn: Machine learning in python. *J. Mach. Learn. Res.*, **12**, 2825–2830.

Peings, Y., 2019: Ural blocking as a driver of early winter stratospheric warmings. *Geophys. Res. Lett.*, **46**, 5460–5468, https://doi.org/10.1029/2019GL082097.

——, and G. Magnusdottir, 2014a: Response of the wintertime Northern Hemisphere atmospheric circulation to current and projected Arctic sea ice decline: A numerical study with CAM5. *J. Climate*, **27**, 244–264, https://doi.org/10.1175/JCLI-D-13-00272.1.

——, and ——, 2014b: Forcing of the wintertime atmospheric circulation by the multidecadal fluctuations of the North Atlantic Ocean. *Environ. Res. Lett.*, **9**, 034018, https://doi.org/10.1088/1748-9326/9/3/034018.

——, and ——, 2016: Wintertime atmospheric response to Atlantic multidecadal variability: Effect of stratospheric representation and ocean–atmosphere coupling. *Climate Dyn.*, **47**, 1029–1047, https://doi.org/10.1007/s00382-015-2887-4.

——, Z. M. Labe, and G. Magnusdottir, 2021: Are 100 ensemble members enough to capture the remote atmospheric response to +2°C Arctic sea ice loss? *J. Climate*, **34**, 3751–3769, https://doi.org/10.1175/JCLI-D-20-0613.1.

Pithan, F., and T. Mauritsen, 2014: Arctic amplification dominated by temperature feedbacks in contemporary climate models. *Nat. Geosci.*, **7**, 181–184, https://doi.org/10.1038/ngeo2071.

Polvani, L. M., and D. W. Waugh, 2004: Upward wave activity flux as a precursor to extreme stratospheric events and subsequent anomalous surface weather regimes. *J. Climate*, **17**, 3548–3554, https://doi.org/10.1175/1520-0442(2004)017<3548:UWAFAA>2.0.CO;2.

——, L. Sun, A. H. Butler, J. H. Richter, and C. Deser, 2017: Distinguishing stratospheric sudden warmings from ENSO as key drivers of wintertime climate variability over the North Atlantic and Eurasia. *J. Climate*, **30**, 1959–1969, https://doi.org/10.1175/JCLI-D-16-0277.1.

Polyak, I., 1996: *Computational Statistics in Climatology*. Oxford University Press, 358 pp.

Previdi, M., K. L. Smith, and L. M. Polvani, 2021: Arctic amplification of climate change: A review of underlying mechanisms. *Environ. Res. Lett.*, **16**, 093003, https://doi.org/10.1088/1748-9326/ac1c29.

Rantanen, M., A. Y. Karpechko, A. Lipponen, K. Nordling, O. Hyvärinen, K. Ruosteenoja, T. Vihma, and A. Laaksonen, 2022: The Arctic has warmed nearly four times faster than the globe since 1979. *Commun. Earth Environ.*, **3**, 168, https://doi.org/10.1038/s43247-022-00498-3.

Rayner, N. A., D. E. Parker, E. B. Horton, C. K. Folland, L. V. Alexander, D. P. Rowell, E. C. Kent, and A. Kaplan, 2003: Global analyses of sea surface temperature, sea ice, and night marine air temperature since the late nineteenth century. *J. Geophys. Res.*, **108**, 4407, https://doi.org/10.1029/2002JD002670.

Romanowsky, E., and Coauthors, 2019: The role of stratospheric ozone for Arctic-midlatitude linkages. *Sci. Rep.*, **9**, 7962, https://doi.org/10.1038/s41598-019-43823-1.

Ronalds, B., E. A. Barnes, R. Eade, Y. Peings, and M. Sigmond, 2020: North Pacific zonal wind response to sea ice loss in the Polar Amplification Model Intercomparison Project and its downstream implications. *Climate Dyn.*, **55**, 1779–1792, https://doi.org/10.1007/s00382-020-05352-w.

Rothrock, D. A., Y. Yu, and G. A. Maykut, 1999: Thinning of the Arctic sea-ice cover. *Geophys. Res. Lett.*, **26**, 3469–3472, https://doi.org/10.1029/1999GL010863.

Rousset, C., and Coauthors, 2015: The Louvain-La-Neuve sea ice model LIM3.6: Global and regional capabilities. *Geosci. Model Dev.*, **8**, 2991–3005, https://doi.org/10.5194/gmd-8-2991-2015.

Ruggieri, P., R. Buizza, and G. Visconti, 2016: On the link between Barents-Kara sea ice variability and European blocking. *J. Geophys. Res. Atmos.*, **121**, 5664–5679, https://doi.org/10.1002/2015JD024021.

Ruprich-Robert, Y., R. Msadek, F. Castruccio, S. Yeager, T. Delworth, and G. Danabasoglu, 2017: Assessing the climate impacts of the observed Atlantic multidecadal variability using the GFDL CM2.1 and NCAR CESM1 global coupled models. *J. Climate*, **30**, 2785–2810, https://doi.org/10.1175/JCLI-D-16-0127.1.

Scinocca, J. F., M. C. Reader, D. A. Plummer, M. Sigmond, P. J. Kushner, T. G. Shepherd, and A. R. Ravishankara, 2009: Impact of sudden Arctic sea-ice loss on stratospheric polar ozone recovery. *Geophys. Res. Lett.*, **36**, L24701, https://doi.org/10.1029/2009GL041239.

Screen, J. A., and J. A. Francis, 2016: Contribution of sea-ice loss to Arctic amplification is regulated by Pacific Ocean decadal variability. *Nat. Climate Change*, **6**, 856–860, https://doi.org/10.1038/nclimate3011.

——, and R. Blackport, 2019a: Is sea-ice-driven Eurasian cooling too weak in models? *Nat. Climate Change*, **9**, 934–936, https://doi.org/10.1038/s41558-019-0635-1.

——, and ——, 2019b: How robust is the atmospheric response to projected Arctic sea ice loss across climate models? *Geophys. Res. Lett.*, **46**, 11 406–11 415, https://doi.org/10.1029/2019GL084936.

——, I. Simmonds, C. Deser, and R. Tomas, 2013: The atmospheric response to three decades of observed Arctic sea ice loss. *J. Climate*, **26**, 1230–1248, https://doi.org/10.1175/JCLI-D-12-00063.1.

——, C. Deser, I. Simmonds, and R. Tomas, 2014: Atmospheric impacts of Arctic sea-ice loss, 1979–2009: Separating forced change from atmospheric internal variability. *Climate Dyn.*, **43**, 333–344, https://doi.org/10.1007/s00382-013-1830-9.

——, and Coauthors, 2018: Consistency and discrepancy in the atmospheric response to Arctic sea-ice loss across climate models. *Nat. Geosci.*, **11**, 155–163, https://doi.org/10.1038/s41561-018-0059-y.

Seierstad, I. A., and J. Bader, 2009: Impact of a projected future Arctic sea ice reduction on extratropical storminess and the NAO. *Climate Dyn.*, **33**, 937–943, https://doi.org/10.1007/s00382-008-0463-x.

Serreze, M. C., and J. A. Francis, 2006: The Arctic amplification debate. *Climatic Change*, **76**, 241–264, https://doi.org/10.1007/s10584-005-9017-y.

——, and J. Stroeve, 2015: Arctic sea ice trends, variability and implications for seasonal ice forecasting. *Philos. Trans. Roy. Soc.*, **A373**, 20140159, https://doi.org/10.1098/rsta.2014.0159.

——, A. P. Barrett, J. C. Stroeve, D. N. Kindig, and M. M. Holland, 2009: The emergence of surface-based Arctic amplification. *Cryosphere*, **3**, 11–19, https://doi.org/10.5194/tc-3-11-2009.

Seviour, W. J. M., 2017: Weakening and shift of the Arctic stratospheric polar vortex: Internal variability or forced response? *Geophys. Res. Lett.*, **44**, 3365–3373, https://doi.org/10.1002/2017GL073071.

Siew, P. Y. F., C. Li, S. P. Sobolowski, and M. P. King, 2020: Intermittency of Arctic–mid-latitude teleconnections: Stratospheric pathway between autumn sea ice and the winter

North Atlantic Oscillation. *Wea. Climate Dyn.*, **1**, 261–275, https://doi.org/10.5194/wcd-1-261-2020.

Simon, A., G. Gastineau, C. Frankignoul, C. Rousset, and F. Codron, 2021: Transient climate response to Arctic sea ice loss with two ice-constraining methods. *J. Climate*, **34**, 3295–3310, https://doi.org/10.1175/JCLI-D-20-0288.1.

——, ——, ——, V. Lapin, and P. Ortega, 2022: Pacific Decadal Oscillation modulates the Arctic sea-ice loss influence on the mid-latitude atmospheric circulation in winter. *Wea. Climate Dyn.*, **3**, 845–861, https://doi.org/10.5194/wcd-3-845-2022.

Simpson, I. R., and Coauthors, 2020: An evaluation of the large-scale atmospheric circulation and its variability in CESM2 and other CMIP models. *J. Geophys. Res. Atmos.*, **125**, e2020JD032835, https://doi.org/10.1029/2020JD032835.

Singarayer, J. S., J. L. Bamber, and P. J. Valdes, 2006: Twenty-first-century climate impacts from a declining Arctic sea ice cover. *J. Climate*, **19**, 1109–1125, https://doi.org/10.1175/JCLI3649.1.

Smith, D. M., N. J. Dunstone, A. A. Scaife, E. K. Fiedler, D. Copsey, and S. C. Hardiman, 2017: Atmospheric response to Arctic and Antarctic sea ice: The importance of ocean–atmosphere coupling and the background state. *J. Climate*, **30**, 4547–4565, https://doi.org/10.1175/JCLI-D-16-0564.1.

——, and Coauthors, 2019: The Polar Amplification Model Intercomparison Project (PAMIP) contribution to CMIP6: Investigating the causes and consequences of polar amplification. *Geosci. Model Dev.*, **12**, 1139–1164, https://doi.org/10.5194/gmd-12-1139-2019.

——, and Coauthors, 2022: Robust but weak winter atmospheric circulation response to future Arctic sea ice loss. *Nat. Commun.*, **13**, 727, https://doi.org/10.1038/s41467-022-28283-y.

Smith, K. L., and P. J. Kushner, 2012: Linear interference and the initiation of extratropical stratosphere-troposphere interactions. *J. Geophys. Res.*, **117**, D13107, https://doi.org/10.1029/2012JD017587.

——, R. R. Neely, D. R. Marsh, and L. M. Polvani, 2014: The Specified Chemistry Whole Atmosphere Community Climate Model (SC-WACCM). *J. Adv. Model. Earth Syst.*, **6**, 883–901, https://doi.org/10.1002/2014MS000346.

——, L. M. Polvani, and L. B. Tremblay, 2018: The impact of stratospheric circulation extremes on minimum Arctic sea ice extent. *J. Climate*, **31**, 7169–7183, https://doi.org/10.1175/JCLI-D-17-0495.1.

Smith, R., and Coauthors, 2010: The Parallel Ocean Program (POP) reference manual, Ocean component of the Community Climate System Model (CCSM) and Community Earth System Model (CESM). LANL Tech. Rep. LAUR-10-01853, 141 pp., https://www2.cesm.ucar.edu/models/cesm1.2/pop2/doc/sci/POPRefManual.pdf.

Streffing, J., T. Semmler, L. Zampieri, and T. Jung, 2021: Response of Northern Hemisphere weather and climate to Arctic sea ice decline: Resolution independence in Polar Amplification Model Intercomparison Project (PAMIP) simulations. *J. Climate*, **34**, 8445–8457, https://doi.org/10.1175/JCLI-D-19-1005.1.

Strey, S. T., W. L. Chapman, and J. E. Walsh, 2010: The 2007 sea ice minimum: Impacts on the Northern Hemisphere atmosphere in late autumn and early winter. *J. Geophys. Res.*, **115**, D23103, https://doi.org/10.1029/2009JD013294.

Stroeve, J., and D. Notz, 2018: Changing state of Arctic sea ice across all seasons. *Environ. Res. Lett.*, **13**, 103001, https://doi.org/10.1088/1748-9326/aade56.

——, T. Markus, L. Boisvert, J. Miller, and A. Barrett, 2014: Changes in Arctic melt season and implications for sea ice loss. *Geophys. Res. Lett.*, **41**, 1216–1225, https://doi.org/10.1002/2013GL058951.

Sun, C., F. Kucharski, J. Li, F.-F. Jin, I.-S. Kang, and R. Ding, 2017: Western tropical Pacific multidecadal variability forced by the Atlantic multidecadal oscillation. *Nat. Commun.*, **8**, 15998, https://doi.org/10.1038/ncomms15998.

Sun, L., C. Deser, L. Polvani, and R. Tomas, 2014: Influence of projected Arctic sea ice loss on polar stratospheric ozone and circulation in spring. *Environ. Res. Lett.*, **9**, 084016, https://doi.org/10.1088/1748-9326/9/8/084016.

——, ——, and R. A. Tomas, 2015: Mechanisms of stratospheric and tropospheric circulation response to projected Arctic sea ice loss. *J. Climate*, **28**, 7824–7845, https://doi.org/10.1175/JCLI-D-15-0169.1.

——, ——, I. Simpson, and M. Sigmond, 2022: Uncertainty in the winter tropospheric response to Arctic sea ice loss: The role of stratospheric polar vortex internal variability. *J. Climate*, **35**, 3109–3130, https://doi.org/10.1175/JCLI-D-21-0543.1.

Suo, L., and Coauthors, 2022a: Simulated contribution of the Interdecadal Pacific Oscillation to the West Eurasia cooling in 1998–2013. *Environ. Res. Lett.*, **17**, 094021, https://doi.org/10.1088/1748-9326/ac88e5.

——, and Coauthors, 2022b: Arctic troposphere warming driven by external radiative forcing and modulated by the Pacific and Atlantic. *J. Geophys. Res. Atmos.*, **127**, e2022JD036679, https://doi.org/10.1029/2022JD036679.

Svendsen, L., N. Keenlyside, I. Bethke, Y. Gao, and N.-E. Omrani, 2018: Pacific contribution to the early twentieth-century warming in the Arctic. *Nat. Climate Change*, **8**, 793–797, https://doi.org/10.1038/s41558-018-0247-1.

Taylor, P. C., and Coauthors, 2021: Process drivers, inter-model spread, and the path forward: A review of amplified Arctic warming. *Front. Earth Sci.*, **9**, 758361, https://doi.org/10.3389/feart.2021.758361.

Thompson, D. W. J., and J. M. Wallace, 2000: Annular modes in the extratropical circulation. Part I: Month-to-month variability. *J. Climate*, **13**, 1000–1016, https://doi.org/10.1175/1520-0442(2000)013<1000:AMITEC>2.0.CO;2.

Tokinaga, H., S.-P. Xie, and H. Mukougawa, 2017: Early 20th-century Arctic warming intensified by Pacific and Atlantic multidecadal variability. *Proc. Natl. Acad. Sci. USA*, **114**, 6227–6232, https://doi.org/10.1073/pnas.1615880114.

Vancoppenolle, M., T. Fichefet, H. Goosse, S. Bouillon, G. Madec, and M. A. Morales Maqueda, 2009: Simulating the mass balance and salinity of Arctic and Antarctic sea ice. 1. Model description and validation. *Ocean Modell.*, **27**, 33–53, https://doi.org/10.1016/j.ocemod.2008.10.005.

Wettstein, J. J., and C. Deser, 2014: Internal variability in projections of twenty-first-century Arctic sea ice loss: Role of the large-scale atmospheric circulation. *J. Climate*, **27**, 527–550, https://doi.org/10.1175/JCLI-D-12-00839.1.

Wilks, D. S., 2016: "The stippling shows statistically significant grid points": How research results are routinely overstated and overinterpreted, and what to do about it. *Bull. Amer. Meteor. Soc.*, **97**, 2263–2273, https://doi.org/10.1175/BAMS-D-15-00267.1.

Woo, S.-H., M.-K. Sung, S.-W. Son, and J.-S. Kug, 2015: Connection between weak stratospheric vortex events and the Pacific decadal oscillation. *Climate Dyn.*, **45**, 3481–3492, https://doi.org/10.1007/s00382-015-2551-z.

Wu, Y., and K. L. Smith, 2016: Response of Northern Hemisphere midlatitude circulation to Arctic amplification in a

simple atmospheric general circulation model. *J. Climate*, **29**, 2041–2058, https://doi.org/10.1175/JCLI-D-15-0602.1.

Wu, Y.-T., Y.-C. Liang, Y.-N. Kuo, F. Lehner, M. Previdi, L. M. Polvani, M.-H. Lo, and C.-W. Lan, 2023: Exploiting SMILEs and the CMIP5 archive to understand Arctic climate change seasonality and uncertainty. *Geophys. Res. Lett.*, **50**, e2022GL100745, https://doi.org/10.1029/2022GL100745.

Xu, M., W. Tian, J. Zhang, J. A. Screen, J. Huang, K. Qie, and T. Wang, 2021: Distinct tropospheric and stratospheric mechanisms linking historical Barents-Kara sea-ice loss and late winter Eurasian temperature variability. *Geophys. Res. Lett.*, **48**, e2021GL095262, https://doi.org/10.1029/2021GL095262.

——, ——, ——, ——, C. Zhang, and Z. Wang, 2023: Important role of stratosphere-troposphere coupling in the Arctic mid-to-upper tropospheric warming in response to sea-ice loss. *npj Climate Atmos. Sci.*, **6**, 9, https://doi.org/10.1038/s41612-023-00333-2.

Zappa, G., P. Ceppi, and T. G. Shepherd, 2021: Eurasian cooling in response to Arctic sea-ice loss is not proved by maximum covariance analysis. *Nat. Climate Change*, **11**, 106–108, https://doi.org/10.1038/s41558-020-00982-8.

Zhang, C., J. Zhang, M. Xu, S. Zhao, and X. Xia, 2022: Impacts of stratospheric polar vortex shift on the East Asian trough. *J. Climate*, **35**, 5605–5621, https://doi.org/10.1175/JCLI-D-21-0235.1.

Zhang, J., and Coauthors, 2022: Responses of Arctic sea ice to stratospheric ozone depletion. *Sci. Bull.*, **67**, 1182–1190, https://doi.org/10.1016/j.scib.2022.03.015.

Zhang, P., Y. Wu, I. R. Simpson, K. L. Smith, X. Zhang, B. De, and P. Callaghan, 2018: A stratospheric pathway linking a colder Siberia to Barents-Kara sea ice loss. *Sci. Adv.*, **4**, eaat6025, https://doi.org/10.1126/sciadv.aat6025.

Zhang, R., and J. A. Screen, 2021: Diverse Eurasian winter temperature responses to Barents-Kara sea ice anomalies of different magnitudes and seasonality. *Geophys. Res. Lett.*, **48**, e2021GL092726, https://doi.org/10.1029/2021GL092726.

——, R. Sutton, G. Danabasoglu, Y.-O. Kwon, R. Marsh, S. G. Yeager, D. E. Amrhein, and C. M. Little, 2019: A review of the role of the Atlantic meridional overturning circulation in Atlantic multidecadal variability and associated climate impacts. *Rev. Geophys.*, **57**, 316–375, https://doi.org/10.1029/2019RG000644.

Zhou, S.-N., Y.-C. Liang, I. Mitevski, and L. M. Polvani, 2023: Stronger Arctic amplification produced by decreasing, not increasing, CO_2 concentrations. *Environ. Res. Climate*, **2**, 045001, https://doi.org/10.1088/2752-5295/aceea2.

Zou, Y., P. J. Rasch, H. Wang, Z. Xie, and R. Zhang, 2021: Increasing large wildfires over the western United States linked to diminishing sea ice in the Arctic. *Nat. Commun.*, **12**, 6048, https://doi.org/10.1038/s41467-021-26232-9.